

Discontinuous Galerkin methods for the Laplace-Beltrami operator on point cloud

GUOZHI DONG^{1,2}, HAILONG GUO³, AND ZUOQIANG SHI^{4,5}

¹Institute for Mathematics, Humboldt University of Berlin, Unter den Linden 6, 10099 Berlin, Germany

²Weierstrass Institute for Applied Analysis and Stochastics, Mohrenstrass 39, 10117 Berlin, Germany

³School of Mathematics and Statistics, The University of Melbourne, Parkville, VIC, 3010, Australia

⁴Department of Mathematical Sciences, Tsinghua University, Beijing, 100084, China

⁵Yanqi Lake Beijing Institute of Mathematical Sciences and Applications, Beijing, 101408, China

Abstract

This paper is delicate to the development of high-order numerical algorithms for solving partial differential equations on point clouds. We introduce a new geometric error analysis framework which requires neither global continuity of surface patches nor exact geometric information, e.g., embedding maps, tangent spaces. The new framework provides us a fundamental tool to analyze discontinuous Galerkin (DG) methods for the Laplace-Beltrami operator on point clouds. It is illustrated using examples of an interior penalty DG method for solving the Laplace-Beltrami equation and the corresponding eigenvalue problem with numerical verification.

AMS subject classifications. 65D18, 65N12, 65N25, 65N30, 68U05

Keywords. Geometric approximation error, discontinuous Galerkin methods, point cloud, Laplace-Beltrami operator, eigenvalue problem

1 Introduction

In recent years, there has been a surge of interest in the study of partial differential equations (PDEs) on manifolds and their numerical methods. Since the seminal work of Dziuk [20], the surface finite element method (SFEM) has been developed into a rich research direction in numerical analysis, see for instance the survey papers [10, 12, 22] and the references therein. Numerical methods for PDEs on manifolds typically involve two levels of discretization (or approximation): one is the discretization of the geometry and its differential structures; the other one is the discretization of the functions defined on the geometry. The greater part of the literature on SFEM seems to have been based on fact that the underlying geometry (manifolds) are surfaces represented by level set functions (e.g., sign distance functions). The geometry approximations are usually limited to continuous piecewise polynomial patches which interpolate underlying smooth manifolds. Using this idea, many of the well known numerical methods in planar domains have been generalized to curved spaces or even evolving manifolds. Exemplary works include SFEM, finite volume method, Crouzeix-Raviart element and so on [15, 19, 21, 23, 24, 31]. Along the same line, discontinuous Galerkin (DG) methods with respect to continuously interpolated piecewise polynomial surfaces have been investigated as well [5, 13, 14]. The vast majority of the geometric error estimations in the existing works are based on the fundamental results of [20] for linear SFEM and [15] for higher-order ones, which are for interpolation type discretizations. In other words, the geometric

errors are interpreted as residuals of local polynomial interpolations. In addition, for computational convenience, most of the existing works deal with the surface gradient and other differential operators based on the explicit tangential projection from the ambient space onto the tangent spaces of the manifolds. That means explicit embedding (e.g., through level set functions) of the manifolds into their ambient Euclidean spaces are assumed to be known. These assumptions are not always satisfied as for the problems we are going to study in this paper, where manifolds are discretized as point clouds. Therefore, the existing theory can not apply directly, and numerical methods for solving PDEs on such type discretized manifolds need to be developed and analyzed.

With the revolutionary development of digital technologies, point cloud becomes a standard and easy way of sampling surfaces in many real-world applications. Due to the discrete nature of point clouds, the existing numerical methods for solving PDEs on point clouds are typically meshfree methods, to name just a few [28,29]. The method in [29] is based on local polynomial approximation of the surface. The idea is natural and easy to implement, but it is difficult to conduct theoretical analysis. The point integral method proposed in [28] was proved to be convergent while the convergence rate is low. In this paper, we are aiming at developing high-order numerical methods to solve PDEs on point clouds with solid theoretical analysis. To get a high order numerical method, first, we need a high order approximation of the underlying surface. Since the surface is given by unstructured point clouds, it is difficult to get a global high order representation. However, it is relatively easy to compute local high order approximations to the surface by polynomial fitting. But, in general, such local approximations may be inconsistent with each other, i.e., the local patches may be discontinuous. Based on the discontinuous geometric representation, the discontinuous Galerkin (DG) method becomes a natural choice. Another difficulty lies in the theoretical error analysis. The geometric assumptions from existing results are violated in this setting. Thus it calls for new ideas in both algorithm designing and numerical analysis for such problems.

In the recent works in [17,18], the idea of using the Riemannian metric tensor for post-processing and analyzing geometric errors has been employed in gradient recovery (post-processing of numerical solutions) and tangential vector fields computation on manifolds with linear SFEM, which turns out to be successful. This motivates us to further develop the ideas in [17,18] to higher-order SFEMs and DG methods, and to a priori error analysis. In this paper, we take the Laplace-Beltrami equations and their corresponding eigenvalue problems as background models. Different from the analysis methods widely adopted in the literature, we take an intrinsic viewpoint. By directly estimating the approximation error of the Riemannian metric tensors, the error analysis of numerical solutions, particularly for the geometric errors, becomes more transparent in comparison to existing results. Instead of working on an abstract unified DG framework as in [2, 5], we concentrate on the so-called interior penalty DG method [6, 16, 25, 32] for solving the mentioned two representative problems. Notice that convergence rates of DG methods for eigenvalue problems on planar domain have been studied, e.g., in [4], and higher-order SFEMs for eigenvalue problems were proposed and analyzed in [11]. Especially, it was observed in [11] that there is a non-synchronization phenomenon between the geometric error and the function approximation error in terms of eigenvalue convergence rates. Whether the error rates in [11] sharp or not was an open question. This paper aims to overcome the above constraints and address the open issues.

Contribution and novelty

The originality of this study is that it presents an algorithmic framework using DG methods for solving elliptical PDEs on point clouds and a brand new generic geometric error analysis tool. The numerical analysis is different from existing methods which are mostly based on the works in [15,20]. Instead, the proposed approach considers approximations of the Riemannian metric tensor of the underlying manifold. The differential operators for functions on manifolds are then represented using local geometric parameterizations and their induced metric tensors. The tangential projection and the explicit embedding maps of the manifolds, which are required in many works in the literature, e.g., [15,20], are not compulsory to know using the new framework. Moreover, it even does not require the surface patches to be continuous, therefore is capable of dealing with more general geometry and allows more flexibility in geometric approximation and numerical methods. This also serves as a starting point for us to study DG methods on point clouds. More explicitly, the error estimate of the metric tensor is established in Theorem 2.9, where a discrepancy phenomenon

between the Jacobian approximation and the metric approximation is reported. In Remark 2.10, an example is provided to justify that our geometric estimates are crucial. These results guide the compatibility of the geometric discretization with the function approximation in order to have optimal convergence rates in numerical methods. Using the intrinsic geometric representation, we are able to design flexible numerical methods and novel error analysis for problems on curved domains. In particular, using the new framework, we prove the convergence rates for high-order DG methods without global continuity of the surface patches in Theorem 3.4. For the numerical analysis of the eigenvalue problem, our approach is also different from both the two works in [4,11]. We show that eigenvalues are invariant under geometric transformations. Then we use the Babuška-Osborn [8] framework and apply it to DG methods on discretized manifolds in Theorem 3.8, which concludes the same theoretical rates as in [11] for high-order SFEMs. Although we focus only on an interior penalty DG (IPDG) method in the analysis and in the numerical examples, our framework and ideas are applicable to other DG methods and SFEMs as well. Last but not least, using a simple example (see Remark 3.9) we argue that the theoretical rates proved in the paper for the convergence of the eigenvalue (therefore also the results in [11]) is actually theoretically optimal.

Structure

The rest of the paper is organized as follows: Section 2 presents an algorithm for patch reconstruction from point clouds and also the geometric error analysis which generalizes the existing results. Section 3 analyzes the convergence rates of numerical solution of the IPDG method for Laplace-Beltrami equation and its eigenvalue problem on point clouds. Finally, the paper is concluded after numerical results and discussions in Section 4. A few technique details are deferred in Appendixes A and B.

2 Geometry reconstruction and its error analysis

In order to develop high-order numerical methods for solving PDEs on point clouds, we need first to reconstruct high-order approximations of the underlying continuous geometry. Therefore, in the following, we outline an algorithm for generating piece-wise smooth patches to approximate the unknown manifold from the point cloud. Error analysis of the reconstructed geometry will be discussed as well. We start with some preliminary on point clouds and manifolds.

2.1 On the point clouds and manifolds

Let Γ be a smooth (sub-)manifold. Let $\Sigma = \{\xi_1, \xi_2, \dots, \xi_N\}$ be set of points which is sampled from the closed smooth (sub-)manifold Γ of known dimension. To make discussions concrete, we consider $\Gamma \subset U \subset \mathbb{R}^3$ as later on in the numerical examples. We also assume there is a closed polyhedral whose faces consist of planar triangles $\{\Omega_h^j\}_{j \in J}$ for some indices set $J \subset \mathbb{N}$. We denote the set of triangle faces $\Omega_h = \bigcup_j \Omega_h^j$. We will abuse a bit of notation in the paper, as later Ω_h^j may denote *both a planar triangle and also the corresponding hyperplane generated from this triangle*. Then there exist some bijective smooth mapping $\pi : \Omega_h \rightarrow \Gamma$. On every Ω_h^j , we build a local coordinate system, so that the origin is in Ω_h^j , and π is a map from \mathbb{R}^2 to \mathbb{R}^3 . This mapping π induces a metric tensor g on Γ through the following relation:

$$g \circ \pi = (\partial\pi)^\top \partial\pi. \quad (2.1)$$

Note that π is not necessarily defined using the global coordinates in \mathbb{R}^3 , but can be alternately defined on every local patch Ω_h^j using the local coordinates on it. We use ∂ to denote the Jacobian, e.g., $\partial\pi \in \mathbb{R}^{3 \times 2}$ is the Jacobian of the geometry map evaluated locally based on the local coordinates on Ω_h^j . It turns out that this relationship is important for the error analysis in this paper.

It is worth noting that the mapping from Ω_h to Γ is not unique. There are infinitely many different choices. However, the metric tensor g is invariant with respect to π . In this paper, we consider the following particular mapping $\pi : \Omega_h \rightarrow \Gamma$ in (2.2):

$$\pi(x) = x - d(x)\nu(x) \quad \text{for every } x \in \Omega_h \text{ in the local coordinates on } \Omega_h, \quad (2.2)$$

where $\nu(x) = \nu(\pi(x))$ is the unit outward normal vector at the point $\pi(x)$ on Γ , and $d(x)$ is the sign distance function of Γ . Note that the expression in (2.2) is coordinate independent. We always consider a patch-wise local coordinate system where the origin is in the face of Ω_h . Particularly, we assume Ω_h to be close enough to Γ , such that the mapping π is bijective between Ω_h^j and $\Gamma_h^j \subset \Gamma$. We use $\Gamma_h := \bigcup_j \Gamma_h^j$ to denote the set of curved triangles on Γ . The Jacobian can be computed by $\partial\pi(x) = P_\tau - d(x)H$, where H is the second fundamental form, whose eigenvalues are the principal curvatures κ of Γ . P_τ is the tangential projection and it satisfies $P_\tau \partial\pi(x) = \partial\pi(x) = \partial\pi(x)P_\tau$.

Provided that $d\kappa < 1$, where κ is the scalar curvature of Γ , we have $\pi : \Omega_h \rightarrow \Gamma_h$ is bijective. To have this fulfilled, we require the distance of Ω_h to Γ_h to be inversely proportional to the curvature. To develop discontinuous Galerkin methods, we shall construct piecewise polynomial patches of order k approximating given point clouds. To be more specific, we use local polynomial function graphs reconstructed from local groups of points and denote such polynomial graph by $\hat{\Gamma}_h^{k,j}$. In Algorithm 1, we provide such a reconstruction from the given point cloud representation of Γ to have $\pi_h^k : \Omega_h \rightarrow \hat{\Gamma}_h^k$. Using the parametrization map π (or π_h^k), the gradient of scalar function on manifolds can be calculated as

$$(\nabla_g v) \circ \pi = \partial\pi(g^{-1} \circ \pi)\nabla\bar{v} \quad \text{or} \quad (\nabla_{g_h^k} v_h^k) \circ \pi_h^k = \partial\pi_h^k((g_h^k)^{-1} \circ \pi_h^k)\nabla\bar{v}_h^k. \quad (2.3)$$

Here $\bar{v} = v \circ \pi$ (or $\bar{v}_h^k = v_h^k \circ \pi_h^k$), and ∇ is the gradient operator on the planar parametric domain Ω_h . Note that this expression of surface gradient is different from the one used in many references for surface finite element methods like [15, 20]. It allows us to develop a brand new numerical analysis framework for investigating PDEs on surfaces or on (sub-)manifolds in general.

2.2 Reference mesh

To get the reference mesh, we first construct an initial triangular mesh $\Omega_H \subset U$. For this initial mesh, we only require that it lies in the reach of the surface such that the map π given in (2.2) is well defined. This requirement is very mild. The initial mesh can be generated easily from point cloud by using surface reconstruction methods, such as screened Poisson reconstruction (SPR) [27], Gauss reconstruction [30] etc. Figure 1 gives an example of the initial triangular mesh constructed by SPR. When the initial mesh is too coarse to be used in the computation, to guarantee an optimal

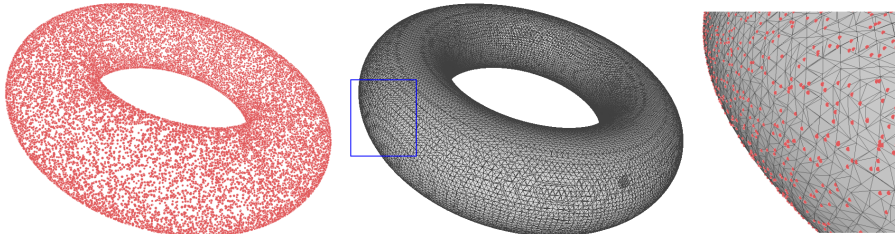


Figure 1: Initial meshes constructed from point cloud. Left: Point cloud; Middle: Reference mesh reconstructed by SPR [27]; Right: Zoom-in of the point cloud and triangular meshes.

convergence rate, we can refine the initial mesh to a satisfactory one. First, for each triangle in the initial mesh, it is refined following the standard procedure until the size of triangles reach the filling distance h_s in Definition 2.1.

Definition 2.1. We call h_s in (2.4) the filling distance of the point cloud Σ

$$h_s := \sup_{\psi \in \Gamma} \min_{\xi \in \Sigma} |\psi - \xi|. \quad (2.4)$$

The refined mesh is denoted as $\tilde{\Omega}_h$. Then, for each nodal point of $\tilde{\Omega}_h$, we find its k -nearest neighbors ($k \geq 3$) in point cloud Σ to fit a hyperplane and project the nodal point to the hyperplane to get a new nodal point. Finally, the reference mesh Ω_h can be obtained by connecting all the new node points. The connections are the same as those in $\tilde{\Omega}_h$. It is easy to check that the reference mesh has the property that

$$\text{dist}(\Omega_h, \Gamma) \sim h_s^2,$$

which will be used in the error analysis to get optimal convergence rate.

2.3 Patch reconstruction from point cloud

Based on the reference mesh obtained in the previous section, we can construct local patch approximations following Algorithm 1.

Algorithm 1 Patch reconstruction from point cloud

Let J is the total number of small triangles of Ω_h . For every $j \in J$, do

- (1) For each Ω_h^j , pick its barycenter c^j , and select a set of m points in Σ which are close to Ω_h^j and uniformly distributed, denoted by $\xi_1^j, \xi_2^j, \dots, \xi_m^j$. Thus $(\xi_i^j)_{i=1, \dots, m}$ is $\mathcal{O}(h^2)$ close to Ω_h^j .
- (2) Let c^j be the origin, and choose a local coordinate system where the hyperplane of Ω_h^j is the transverse plane. Then we change the coordinates of $\{\xi_i^j\}_{i=1}^m$ according to the new local system. In the local coordinates, $\{\xi_i^j\}_{i=1}^m$ is represented as (s_i^j, v_i^j) for $s_i^j \in \Omega_h^j$.
- (3) Then approximate (interpolate) the points using an k^{th} order polynomial function graph defined on the hyperplane of Ω_h^j . That is to find $p_h^{k,j}$ such that

$$p_h^{k,j} = \underset{p}{\operatorname{argmin}} \frac{1}{m} \sum_{i=1}^m |p(s_i^j) - v_i^j|^2 \text{ over } p \in \mathbb{P}^k(\Omega_h^j). \quad (2.5)$$

The number m chosen in the first step is sufficiently large, and the points are distributed uniformly, so that problem (2.5) is well-conditioned.

- (4) Select some interpolating points $(x_k^j)_k \subset \Omega_h^j$ in the parameter domain. Typically, those points x_k^j are chosen according to the polynomial degree.
 - (5) Compute $\psi_k^j = \pi_h^k(x_k^j)$ for those selected points $x_k^j \in \Omega_h^j$ using the iterations described in (2.8) to get the corresponding points ψ_k^j .
 - (6) Interpolate ψ_k^j to get corresponding polynomial patch denoted as $\hat{\Gamma}_h^{k,j}$.
-

Note that $\hat{\Gamma}_h^{k,j}$ consists of piecewise polynomial patches, but no interpolating Γ_h . In Algorithm 1, ψ_k^j is still yet to compute. For a given point $x \in \Omega_h^j$ over the parametric domain, we compute the point $\psi \in \Gamma_h^{k,j}$ such that $\psi(x) - x = -d_h^k(x) \nu_h^{k,j}(x)$, where $\nu_h^{k,j}$ denotes the unit outward normal vector of the local polynomial graph, and d_h^k is the length of the vector $\psi - x$. Since $\psi = (\psi_1, \psi_2, \psi_3)$ is a local polynomial graph, i.e., $\psi_3 = p_h^{k,j}(\psi_1, \psi_2)$, then using this local coordinates, $x = (x_1, x_2, 0)$. Also notice that $d_h^k(x) = \sqrt{(\psi_1 - x_1)^2 + (\psi_2 - x_2)^2 + (\psi_3)^2}$, and $\nu_h^{k,j}(x) = \frac{(-\partial_1 p_h^{k,j}, -\partial_2 p_h^{k,j}, 1)^\top}{\sqrt{(\partial_1 p_h^{k,j})^2 + (\partial_2 p_h^{k,j})^2 + 1}}$.

This gives us the following nonlinear system

$$\begin{aligned} \psi_3 \partial_1 p_h^{k,j}(\psi_1, \psi_2) + \psi_1 - x_1 &= 0 \\ \psi_3 \partial_2 p_h^{k,j}(\psi_1, \psi_2) + \psi_2 - x_2 &= 0 \\ \psi_3 - p_h^{k,j}(\psi_1, \psi_2) &= 0. \end{aligned} \quad (2.6)$$

We rewrite the above system in a compact form as $M(\psi) = 0$ which can then be solved using Newton's method. For that, we reduce the above system to a two-variable equation

$$\begin{aligned} M_1(\psi_1, \psi_2) &= p_h^{k,j}(\psi_1, \psi_2) \partial_1 p_h^{k,j}(\psi_1, \psi_2) + \psi_1 - x_1 = 0 \\ M_2(\psi_1, \psi_2) &= p_h^{k,j}(\psi_1, \psi_2) \partial_2 p_h^{k,j}(\psi_1, \psi_2) + \psi_2 - x_2 = 0. \end{aligned} \quad (2.7)$$

This system then gives rise to the following iterations for some initial guess, e.g., $(\psi_1^0, \psi_2^0)^\top = (x_1, x_2)^\top$:

$$(\psi_1^{m+1}, \psi_2^{m+1})^\top = (\psi_1^m, \psi_2^m)^\top - (\nabla M^m)^{-1} (M_1^m, M_2^m)^\top; \quad \psi_3^{m+1} = p_h^{k,j}(\psi_1^{m+1}, \psi_2^{m+1}), \quad (2.8)$$

where $M_i^m = M_i(\psi_1^m, \psi_2^m)$, and $\nabla M^m = \begin{pmatrix} \partial_1 M_1(\psi_1^m, \psi_2^m) & \partial_1 M_2(\psi_1^m, \psi_2^m) \\ \partial_2 M_1(\psi_1^m, \psi_2^m) & \partial_2 M_2(\psi_1^m, \psi_2^m) \end{pmatrix}$ which is a symmetric matrix. Note that its inverse matrix can be explicitly calculated

$$(\nabla M^m)^{-1} = \frac{1}{\det(\nabla M^m)} \begin{pmatrix} \partial_2 M_2(\psi_1^m, \psi_2^m) & -\partial_1 M_2(\psi_1^m, \psi_2^m) \\ -\partial_2 M_1(\psi_1^m, \psi_2^m) & \partial_1 M_1(\psi_1^m, \psi_2^m) \end{pmatrix}.$$

The Newton iterations are terminated once an expected accuracy level is reached (in our examples, we choose it to be 10^{-14}).

Remark 2.2. We notice here that (4) and (5) are important for the optimal convergence rates of the algorithm. In particular, it is crucial in the geometric error analysis to prove the statement of Proposition 2.6.

2.4 Geometric error analysis

One difficulty in numerical analysis for problems on manifolds is that there are error sources in the discretization of both geometry and functions defined on the geometry. Much of the literature focuses on the case that the geometric error is the local polynomial interpolation residuals. However, in the case of point clouds, this is usually not true. To apply (discontinuous) Galerkin methods, we first reconstruct a set of patches from the point cloud which approximates the original manifold Γ . To proceed with the error analysis, we consider the following notation and assumptions.

Definition 2.3. On every local plane of Ω_h , we decompose all the vectors ξ to be vectors of the form ξ_{Ω_h} and ξ_o , which denote the components projected onto Ω_h and the orthogonal residuals, respectively, i.e.,

$$\xi = \xi_{\Omega_h} + \xi_o, \quad \text{and} \quad \xi_{\Omega_h} \perp \xi_o.$$

Assumption 2.4. We consider the following assumptions throughout the paper.

1. Γ is C^{k_0} smooth, for $k_0 \geq \max\{k, 2\}$, where k is the polynomial order of the surface reconstruction, and its curvature is uniformly bounded.
2. The filling distance h_s in (2.4) is small enough, and $h \geq c_k h_s$ is the largest diameter of the triangles on Ω_h . Here $c_k \geq 1$ is some constant depending on k , which controls the lower bound of h so that the polynomial reconstruction in Algorithm 1 is well-conditioned.
3. Every face of the polyhedral Ω_h is $\mathcal{O}(h^2)$ close to the corresponding patches in Γ_h , and shape regular. This is understood in the sense that for every selected triangle pair Ω_h^j and Γ_h^j , we have $|\pi(x) - x| \leq Ch^2$ with some uniform constant C independent of h and x . Thus the points in the point cloud are also $\mathcal{O}(h^2)$ close to Ω_h in that sense.

The bounded curvature of Γ implies another useful estimate $|\nu_{\Omega_h}| \leq Ch$ as we see in Lemma 2.5. In the next, we do not distinguish the notation Γ and Γ_h .

Lemma 2.5. Let Assumption 2.4 be fulfilled. Let $\Omega_h = \cup_{j \in J} \Omega_h^j$ be the parameter domain where $\pi : \Omega_h \rightarrow \Gamma_h$ is defined as (2.2). If the diameter of every Ω_h^j is of scale $h < 1$, then for every unit normal vector, there exists a constant C independent of h , such that

$$|\nu_{\Omega_h}| \leq Ch \quad \text{where } \nu_{\Omega_h} \text{ is the decomposition of } \nu \text{ given as in Definition 2.3.}$$

Proof. Taking arbitrary two unit normal vectors in the same patch Γ_h^j , let us denote it by $\nu(\xi^a)$ and $\nu(\xi^b)$. The scalar curvature κ being uniformly bounded indicates that there exist some constant $C_\kappa > 0$, such that

$$\sup_{\xi^a \neq \xi^b \in \Gamma_h^j} \frac{|\nu(\xi^a) - \nu(\xi^b)|}{|\xi^a - \xi^b|} \leq C_\kappa.$$

Take the three nodal points (or vertices) of the triangle Ω_h^j , and find their corresponding nodal points on Γ_h^j , which forms another triangle in the plane $\hat{\Omega}_h^j$. Because of the assumed condition that

the triangle in Ω_h^j is $\mathcal{O}(h^2)$ close to Γ_h^j and shape regular, the two outward unit normal vectors of Ω_h^j and $\hat{\Omega}_h^j$, denoted by z_h^j and \hat{z}_h^j , respectively, satisfy the error bounds

$$|z_h^j - \hat{z}_h^j| \leq C_1 h.$$

Let us now fix $\xi_j^b \in \Gamma_h^j$ to be the point at which the unit normal vector is parallel to \hat{z}_h^j . Note that $(z_h^j)_{\Omega_h} = 0$. Then we have $|\nu_{\Omega_h}(\xi_j^b)| \leq |z_h^j - \hat{z}_h^j| \leq C_1 h$, and $\xi - \xi_j^b \leq ch$ for all $\xi \in \Gamma_h^j$. Finally, for every $j \in J$, we derive

$$|\nu_{\Omega_h}(\xi)| \leq |\nu_{\Omega_h}(\xi_j^b)| + |\nu_{\Omega_h}(\xi) - \nu_{\Omega_h}(\xi_j^b)| \leq C_1 h + |\nu(\xi) - \nu(\xi_j^b)| \leq C_1 h + C_\kappa |\xi - \xi_j^b|. \quad (2.9)$$

□

The scaling constant C can be further optimized with respect to the scalar curvature κ , though it is not pursued here. We now show approximation property for the nodal points $(\psi^i)_{i \in \mathbb{N}}$ reconstructed from Algorithm 1. In view of the equation in (2.6), the partial differential operators seem to reduce the approximation accuracy of the polynomial functions p_h^j after the Newton iterations. In the following, we show that surprisingly this is *not* the case as long as the Newton algorithm (2.8) converges sufficiently.

Here and also in the following sections, we always use C to denote some h independent generic constant, which may take different values in different estimates. Now, we are in the position to present a fundamental approximation result.

Proposition 2.6. *Let Assumption 2.4 be satisfied for the point cloud and Γ_h . Suppose the Newton iteration in Algorithm 1 stops with a sufficiently small error. Then the reconstructed nodal points $(\psi^i)_{i \in \mathbb{N}} \subset \hat{\Gamma}_h^k$ satisfy the following approximation property to the precise nodal points $(\xi^i)_{i \in \mathbb{N}} \subset \Gamma$*

$$|\psi^i - \xi^i| \leq Ch^{k+1}. \quad (2.10)$$

In particular,

$$|\psi_{\Omega_h}^i - \xi_{\Omega_h}^i| \leq Ch^{k+2}, \quad (2.11)$$

where $\psi_{\Omega_h}^i$ and $\xi_{\Omega_h}^i$ are the nodal points of ψ^i and ξ^i projected onto the parametric domain Ω_h , respectively.

Before we prove Proposition 2.6, we provide an auxiliary lemma on the polynomial approximation of scattering points. This is a standard result that is available in many references, e.g., [33]. For completeness, a proof is provided in Appendix A.

Lemma 2.7. *Let the local patches be reconstructed as in Algorithm 1, which are function graphs of k^{th} order polynomials, and let Assumption 2.4 be true for the point cloud. Suppose that the selected points are chosen such that the polynomial reconstruction is well-posed for every patch in Algorithm 1. Then, the fitting polynomial function satisfies*

$$\left\| p_h^{k,j} - p^j \right\|_{L^\infty(\Omega_h^j)} \leq Ch^{k+1} \quad \text{and} \quad \left\| \nabla p_h^{k,j} - \nabla p^j \right\|_{L^\infty(\Omega_h^j)} \leq Ch^k \quad \text{for all } j \in J. \quad (2.12)$$

where $p_h^{k,j}$ and p^j are the local polynomial function and the precise function whose graph gives the exact patch on Γ , respectively.

Proof of Proposition 2.6. In the proof, to ease the notation, we ignore all the index j , but keep in mind that we always consider the estimate patch-wise. Recall the formula (2.6). Then we have

$$\psi_{\Omega_h}^i - \xi_{\Omega_h}^i = p(\xi_{\Omega_h}^i) \nabla p(\xi_{\Omega_h}^i) - p_h^k(\psi_{\Omega_h}^i) \nabla p_h^k(\psi_{\Omega_h}^i) \quad \text{and} \quad \psi_o^i - \xi_o^i = p_h^k(\psi_{\Omega_h}^i) - p(\xi_{\Omega_h}^i) \quad (2.13)$$

where $p_h^k : \Omega_h \rightarrow \mathbb{R}$ is the reconstructed local polynomial patch in Algorithm 1, and $p : \Omega_h \rightarrow \mathbb{R}$ is the counterpart of p_h^k associated to the patch on Γ . Note that p and p_h^k satisfy the estimate from Lemma 2.7. In particular, they satisfy the estimates

$$\|p\|_{L^\infty(\Omega_h)} \leq Ch^2 \quad \text{and} \quad \|p_h^k\|_{L^\infty(\Omega_h)} \leq Ch^2. \quad (2.14)$$

To further simplify the presentation, we will ignore the $L^\infty(\Omega_h)$ norm subscript in the rest of the proof. Note that (2.14) and (2.12) together imply that both $\|\nabla p\|$ and $\|\nabla p_h^k\|$ are of order $\mathcal{O}(h)$. Using the triangle inequality, the left equality in (2.13) leads to

$$\begin{aligned} |\psi_{\Omega_h}^i - \xi_{\Omega_h}^i| &\leq \|\nabla p(\xi_{\Omega_h}^i)(p(\xi_{\Omega_h}^i) - p_h^k(\xi_{\Omega_h}^i))\| + \|(p_h^k(\xi_{\Omega_h}^i) - p_h^k(\psi_{\Omega_h}^i))\nabla p(\xi_{\Omega_h}^i)\| \\ &\quad + \|p_h^k(\psi_{\Omega_h}^i)(\nabla p(\xi_{\Omega_h}^i) - \nabla p_h^k(\xi_{\Omega_h}^i))\| + \|p_h^k(\psi_{\Omega_h}^i)(\nabla p_h^k(\xi_{\Omega_h}^i) - \nabla p_h^k(\psi_{\Omega_h}^i))\| \\ &\leq \|\nabla p(\xi_{\Omega_h}^i)\| \|p(\xi_{\Omega_h}^i) - p_h^k(\xi_{\Omega_h}^i)\| + L \|\psi_{\Omega_h}^i - \xi_{\Omega_h}^i\| \|\nabla p(\xi_{\Omega_h}^i)\| \\ &\quad + \|p_h^k(\psi_{\Omega_h}^i)\| \|\nabla p(\xi_{\Omega_h}^i) - \nabla p_h^k(\xi_{\Omega_h}^i)\| + L' \|\psi_{\Omega_h}^i - \xi_{\Omega_h}^i\| \|p_h^k(\psi_{\Omega_h}^i)\|, \end{aligned}$$

where L and L' are the local Lipschitz constants of the polynomial functions p_h^k and ∇p_h^k over Ω_h , respectively. Particularly the magnitudes of L and L' are of order $\mathcal{O}(h)$ and $\mathcal{O}(1)$, respectively, thus uniformly bounded. Rearranging the above inequality, we have

$$\begin{aligned} &(1 - L \|\nabla p(\xi_{\Omega_h}^i)\| - L' \|p_h^k(\psi_{\Omega_h}^i)\|) \|\psi_{\Omega_h}^i - \xi_{\Omega_h}^i\| \\ &\leq \|\nabla p(\xi_{\Omega_h}^i)\| \|p(\xi_{\Omega_h}^i) - p_h^k(\xi_{\Omega_h}^i)\| + \|p_h^k(\psi_{\Omega_h}^i)\| \|\nabla p(\xi_{\Omega_h}^i) - \nabla p_h^k(\xi_{\Omega_h}^i)\| \end{aligned}$$

The above inequality tells that for sufficiently small h_0 , there exists a constant C such that

$$0 < C \leq (1 - L \|\nabla p(\xi_{\Omega_h}^i)\| - L' \|p_h^k(\psi_{\Omega_h}^i)\|) \quad \text{for all } h \leq h_0.$$

Then we have

$$\begin{aligned} &|\psi_{\Omega_h}^i - \xi_{\Omega_h}^i| \\ &\leq \frac{1}{C} (\|\nabla p(\xi_{\Omega_h}^i)\| \|p(\xi_{\Omega_h}^i) - p_h^k(\xi_{\Omega_h}^i)\| + \|p_h^k(\psi_{\Omega_h}^i)\| \|\nabla p(\xi_{\Omega_h}^i) - \nabla p_h^k(\xi_{\Omega_h}^i)\|) \end{aligned}$$

which together with (2.12) and (2.14) confirm (2.11), i.e., $\|\psi_{\Omega_h}^i - \xi_{\Omega_h}^i\| \leq Ch^{k+2}$. Back to the second part of (2.13), similarly we have

$$|\psi_o^i - \xi_o^i| \leq \|p_h^k(\psi_{\Omega_h}^i) - p(\psi_{\Omega_h}^i)\| + \|p(\psi_{\Omega_h}^i) - p(\xi_{\Omega_h}^i)\| \leq Ch^{k+1} + L \|\psi_{\Omega_h}^i - \xi_{\Omega_h}^i\|.$$

This concludes the statement in (2.10) by noticing that

$$|\psi^i - \xi^i| \leq |\psi_o^i - \xi_o^i| + |\psi_{\Omega_h}^i - \xi_{\Omega_h}^i|.$$

□

The error bounds (2.10) and (2.11) enable us to estimate further the geometric approximation errors. *We remark that for continuous interpolated patches, the error in Proposition 2.6 vanishes.* Recall Definition 2.3, due to the linearity of the Jacobian we immediately have

$$\partial\pi = (\partial\pi)_o + (\partial\pi)_{\Omega_h} \quad \text{and} \quad \partial\pi_h^k = (\partial\pi_h^k)_o + (\partial\pi_h^k)_{\Omega_h}.$$

Lemma 2.8. *Let the same assumptions as Proposition 2.6 hold. Let $\pi : \Omega_h \rightarrow \Gamma_h$ and $\pi_h^k : \Omega_h \rightarrow \hat{\Gamma}_h^k$ be the mapping associated to the original patches on Γ and the reconstructed polynomial patches, respectively. The reconstruction is done by interpolating the reconstructed nodal points from Algorithm 1. Then we have the following error bounds:*

$$\begin{aligned} \|\partial\pi - \partial\pi_h^k\|_{L^\infty(\Omega_h)} &\leq Ch^k, \quad \left\| (\partial\pi - \partial\pi_h^k)_{\Omega_h} \right\|_{L^\infty(\Omega_h)} \leq Ch^{k+1}, \\ \left\| (\partial\pi_h^k)_o \right\|_{L^\infty(\Omega_h)} &\leq Ch \quad \text{and} \quad \left\| (\partial\pi)_o \right\|_{L^\infty(\Omega_h)} \leq Ch. \end{aligned} \tag{2.15}$$

Proof. Based on Lemma 2.7, and let $\tilde{\pi}_h^k$ be the polynomial patch by interpolating the exact nodal points $\{\xi^i\}$. Therefore we have that $\tilde{\pi}_h^k = \sum_{i=1}^m \xi^i \phi_i$ and $\pi_h^k = \sum_{i=1}^m \psi^i \phi_i$ where m is the number of nodal points depending on the interpolating polynomial orders, and $(\phi_i)_i$ are the Lagrange polynomial bases. This shows that

$$\|\partial\tilde{\pi}_h^k - \partial\pi_h^k\|_{L^\infty(\Omega_h)} \leq Ch^k.$$

To see the first estimate in (2.15), we simply use the triangle inequality and the interpolation error bounds to derive

$$\|\partial\pi - \partial\pi_h^k\|_{L^\infty(\Omega_h)} \leq \|\partial\pi - \partial\tilde{\pi}_h^k\|_{L^\infty(\Omega_h)} + \|\partial\tilde{\pi}_h^k - \partial\pi_h^k\|_{L^\infty(\Omega_h)} \leq C_1 h^k.$$

For the second estimate in (2.15), notice that $(\partial\tilde{\pi}_h^k - \partial\pi_h^k)_{\Omega_h} = \sum_{i=1}^m (\psi_{\Omega_h}^i - \xi_{\Omega_h}^i)\phi_i$. Then by the triangle inequality we have

$$\|(\partial\pi - \partial\pi_h^k)_{\Omega_h}\|_{L^\infty(\Omega_h)} \leq \|(\partial\pi - \partial\tilde{\pi}_h^k)_{\Omega_h}\|_{L^\infty(\Omega_h)} + \|(\partial\tilde{\pi}_h^k - \partial\pi_h^k)_{\Omega_h}\|_{L^\infty(\Omega_h)}. \quad (2.16)$$

For the first term on the right hand side of (2.16), we notice that $\pi - \tilde{\pi}_h^k = (d_h^k)\nu$, where $|d_h^k| \leq c_1 h^{k+1}$ (c.f. [15]) is the distances of points from $\tilde{\pi}_h^k$ to π along the normal vector ν . Due to Lemma 2.5, we have that on every local patch Ω_h^j , $|(\nu)_{\Omega_h^j}| \leq Ch$. Then using product rule and the triangle inequality we have

$$\begin{aligned} \|(\partial\pi - \partial\tilde{\pi}_h^k)_{\Omega_h}\|_{L^\infty(\Omega_h)} &= \left\| \partial(d_h^k \nu_{\Omega_h}) \right\|_{L^\infty(\Omega_h)} \\ &\leq Ch \left\| (d_h^k)' \right\|_{L^\infty(\Omega_h)} + c_1 h^{k+1} \|(\partial\nu)_{\Omega_h}\|_{L^\infty(\Omega_h)} = \mathcal{O}(h^{k+1}). \end{aligned}$$

Note that $(\partial\nu)_{\Omega_h}$ is again bounded by curvature. The second term on the right hand side of (2.16) can be estimated from (2.11). These together confirm the conclusion. The third and the fourth estimates follow from the fact that, for every fixed index i , ψ_o^i and ξ_o^i are both of $\mathcal{O}(h^2)$ distance to their corresponding parametric domain Ω_h . \square

To simplify notations, we will not distinguish metric tensors g and g_h^k with $g \circ \pi$ and $g_h^k \circ \pi_h^k$ in the following. In Theorem 2.9, we show a surprising result that the metric tensor resulted from the reconstructed polynomial patch has one order higher accuracy than the Jacobian approximation (compare to Lemma 2.8).

Theorem 2.9. *Given the same condition as Lemma 2.8, we have*

$$\begin{aligned} \|g^{-1}(g - g_h^k)\|_{L^\infty} &\leq Ch^{k+1}, \quad \left\| \frac{\sqrt{|g|} - \sqrt{|g_h^k|}}{\sqrt{|g|}} \right\|_{L^\infty} \leq Ch^{k+1}, \\ \left\| \frac{l_{g_h^k} - l_g}{l_g} \right\|_{L^\infty} &\leq Ch^{k+1} \quad \text{and} \quad \|g^{-1}(\partial\pi)^\top n - (g_h^k)^{-1}(\partial\pi_h^k)^\top n_h^k\|_{L^\infty} \leq Ch^{k+1}, \end{aligned} \quad (2.17)$$

where n and n_h^k are the unit normal vectors on the edges of the curved triangles, which are tangential to the surfaces Γ and $\hat{\Gamma}_h^k$, respectively.

Proof. Recall that $g \circ \pi = (\partial\pi)^\top \partial\pi$, and $g_h^k \circ \pi_h^k = (\partial\pi_h^k)^\top \partial\pi_h^k$. Note that all the quantities in (2.17) are independent of the local coordinate system, therefore, we choose both π and π_h^k are function graphs on Ω_h . In this case $(\partial\pi)_{\Omega_h}$ and $(\partial\pi)_o$ are orthogonal, and the same holds for π_h^k . Then we have

$$\begin{aligned} g^{-1}(g - g_h^k) &= g^{-1}((\partial\pi)^\top \partial\pi - (\partial\pi_h^k)^\top \partial\pi_h^k) \\ &= g^{-1} \frac{1}{2} (((\partial\pi)^\top + (\partial\pi_h^k)^\top)(\partial\pi - \partial\pi_h^k) + ((\partial\pi)^\top - (\partial\pi_h^k)^\top)(\partial\pi + \partial\pi_h^k)) \\ &= g^{-1} \frac{1}{2} (((\partial\pi)^\top + (\partial\pi_h^k)^\top)_{\Omega_h}(\partial\pi - \partial\pi_h^k)_{\Omega_h} + ((\partial\pi)^\top - (\partial\pi_h^k)^\top)_{\Omega_h}(\partial\pi + \partial\pi_h^k)_{\Omega_h}) \\ &\quad + g^{-1} \frac{1}{2} (((\partial\pi)^\top + (\partial\pi_h^k)^\top)_o(\partial\pi - \partial\pi_h^k)_o + ((\partial\pi)^\top - (\partial\pi_h^k)^\top)_o(\partial\pi + \partial\pi_h^k)_o) \end{aligned}$$

where we use the decomposition in Definition 2.3. Note that due to the assumptions on Γ , g^{-1} is uniformly bounded independent of h . Then using the estimate from Lemma 2.8, we have the following

$$\|(\partial\pi - \partial\pi_h^k)_{\Omega_h}\|_{L^\infty(\Omega_h)} \leq Ch^{k+1} \quad \text{and} \quad \|((\partial\pi)^\top - (\partial\pi_h^k)^\top)_o\|_{L^\infty(\Omega_h)} \leq Ch^k$$

and $\|(\partial\pi + \partial\pi_h^k)_{\Omega_h}\|_{L^\infty(\Omega_h)} \leq C$ is uniformly bounded for some constant C independent of h and

$$\|((\partial\pi)^\top + (\partial\pi_h^k)^\top)_o\|_{L^\infty(\Omega_h)} \leq Ch.$$

These together give us the first estimate. The second and the third estimates are consequences derived immediately from the first estimate. We skip the details here. For the fourth one, notice that $n = \partial\pi e_n$ and $n_h^k = \partial\pi_h^k e_{n_h}$ where e_n and e_{n_h} both are 2×1 vectors defined on the edges of the triangles in the common planar parameter domain Ω_h . Since both Γ_h and $\hat{\Gamma}_h^k$ have uniformly bounded curvature, then the lengths of e_n and e_{n_h} are uniformly bounded from above and also bounded away from zero. Thus

$$g^{-1}(\partial\pi)^\top n - (g_h^k)^{-1}(\partial\pi_h^k)^\top n_h^k = g^{-1}g e_n - (g_h^k)^{-1}g_h^k e_{n_h} = e_n - e_{n_h}.$$

On the other hand, due to the fact that n and n_h are unitary vectors, and g is positive definite, we have

$$e_n^\top g e_n = e_{n_h}^\top g_h^k e_{n_h} = 1 \quad \Rightarrow \quad (e_n - e_{n_h})^\top g (e_n + e_{n_h}) = e_{n_h}^\top (g_h^k - g) e_{n_h}$$

Due to the positive definiteness of the metric tensor g , the above relation indicates that

$$\|e_n - e_{n_h}\|_{L^\infty(\Omega_h)} \leq C \|g - g_h^k\|_{L^\infty}$$

which then gives us the estimate that

$$\|g^{-1}(\partial\pi)^\top n - (g_h^k)^{-1}(\partial\pi_h^k)^\top n_h^k\|_{L^\infty(\Omega_h)} = \|e_n - e_{n_h}\|_{L^\infty(\Omega_h)} = \mathcal{O}(h^{k+1}).$$

□

Remark 2.10. We note that surprisingly the two error estimates of the Jacobian $\|\partial\pi - \partial\pi_h^k\|_{L^\infty(\Omega_h)}$ and the metric tensors $\|g - g_h^k\|_{L^\infty}$ are not of the same order, even though the metric tensors are represented by product of Jacobian and its transpose given in (2.1). The extra order for the metric tensor approximation is due to the assumption that the local patches parameterized by Ω_h are in the $\mathcal{O}(h^2)$ neighborhood of Ω_h , which results in the estimate in (2.11). For the interpolating polynomial patches of a smooth manifold as in the literature, (2.11) is automatically fulfilled. However, it is not granted for arbitrary approximations. Notice that, with only the condition (2.10), it is in general not sufficient to prove the results in Theorem 2.9. For the interpolating polynomial patches of a smooth manifold as in the literature, (2.11) is automatically fulfilled, which seems to be not granted for arbitrary approximations. Notice that, with only the condition (2.10), it is in general not sufficient to prove the results in Theorem 2.9. An immediate example one may think is a right-angled triangle with two orthogonal edges of length h , while another right-angled triangle in the same plane with two orthogonal edges of length $h + h^{k+1}$. For such a pair, (2.10) is satisfied but not (2.11). Then the ratio of the areas of the two triangles is $1 + 2h^k + h^{k+1}$, i.e., $\left\| \frac{\sqrt{|g|} - \sqrt{|g_h^k|}}{\sqrt{|g|}} \right\|_{L^\infty} = 2h^k + h^{k+1}$ for these two patches, which does not give the results in Theorem 2.9. This also explains that the closeness property (2.11) in Proposition 2.6 for Algorithm 1 is crucial.

Remark 2.11. The result of Proposition 2.6 implies that to have the same error bounds in Theorem 2.9, it is not necessary to require the points from the point cloud to be on the exact manifold. We believe that (2.10) and (2.11) are the sufficient conditions to derive the error bounds of the metric tensors in such cases.

3 DG methods in curved domain and their error analysis

To illustrate the main idea better, we focus on two important exemplary elliptical PDEs on Γ . The first one is the Laplace-Beltrami equation: Given $f \in L^2(\Gamma)$, find $u \in H^2(\Gamma)$ such that

$$-\Delta_g u + u = f, \quad (3.1)$$

where g is the Riemannian metric of Γ . The weak version of problem (3.1) is to find $u \in H^1(\Gamma)$ such that

$$\mathcal{A}(u, v) = (f, v), \quad \text{for all } v \in H^1(\Gamma). \quad (3.2)$$

where

$$\mathcal{A}(u, v) = \int_{\Gamma} (\nabla_g u \cdot \nabla_g v + uv) dA_g, \quad \text{and} \quad (f, v) = \int_{\Gamma} f v dA_g.$$

The second model equation is the eigenvalue problem associated to the Laplace-Beltrami operator on Γ : find pairs $(\lambda, u) \in (\mathbb{R}^+, H^2(\Gamma))$ such that

$$-\Delta_g u = \lambda u. \quad (3.3)$$

The eigenvalues are assumed to be ordered so that $0 = \lambda_1 \leq \lambda_2 \leq \dots \leq \lambda_n \leq \dots$, and the corresponding eigenfunctions are normalized to satisfy $\|u_i\|_{L^2(\Gamma)} = 1$. The weak formulation of (3.3) read as: find $(\lambda, u) \in (\mathbb{R}^+, H^1(\Gamma))$ with $\|u\|_{L^2(\Gamma)} = 1$ such that

$$\int_{\Gamma} \nabla_g u \cdot \nabla_g v dA_g = \lambda \int_{\Gamma} u v dA_g \quad \text{for all } v \in H^1(\Gamma). \quad (3.4)$$

Well-posedness of the above problems have been discussed for instance in [7]. Our goal here is to develop numerical methods for such type of PDEs when Γ is given in the form of point cloud sampling.

3.1 DG methods for PDEs on curved domain

In this paper, we shall focus on an interior penalty discontinuous Galerkin method (IPDG) for PDEs on point cloud.

The standard formulations of DG methods in a surface setting have been studied in [5, 14], a bilinear form of which is recalled as follows:

$$\begin{aligned} \mathcal{A}_h^{k,l}(u_h, v_h) := & \sum_j \int_{\hat{\Gamma}_h^{k,j}} (\nabla_{g_h^k} u_h \cdot \nabla_{g_h^k} v_h + u_h v_h) dA_{g_h^k} \\ & - \sum_{\hat{e}_h^k \in \hat{\mathcal{E}}_h} \int_{\hat{e}_h^k} \left(\{(\nabla_{g_h^k} u_h \cdot n_h)\}[v_h] + \{(\nabla_{g_h^k} v_h \cdot n_h)\}[u_h] - \frac{\beta}{h}[u_h][v_h] \right) dE_{g_h^k}. \end{aligned} \quad (3.5)$$

Here $\hat{\mathcal{E}}_h$ denotes the edge set contains all the edges from the curved triangle faces in $\hat{\Gamma}_h^k$, β denotes the stabilization parameter, and n_h is the out unit normal vector orthogonal to the edges \hat{e}_h^k and tangential to $\hat{\Gamma}_h^k$. For quantity q defined on $(\hat{e}_h^{k,j})^\pm \in \partial \hat{\Gamma}_h^{k,j}$, the averaging is defined to be $\{q\} := \frac{1}{2}(q^+ + q^-)$ and the jump is defined to be $[q] := q^+ - q^-$. The main difference is that in [5], the exact manifolds are assumed to be known and $\hat{\Gamma}_h^k$ is assumed to be piecewise polynomial interpolation of Γ_h . However, different situations are confronted in general for point clouds. First of all, Γ is not known, and thus $\hat{\Gamma}_h^k$ is not immediately available for given point clouds. We need to construct such an approximation from a set of scattered points in order to apply a Galerkin type numerical method. This shall be discussed in Section 2.3. Secondly, it might be the case that the reconstructed patches share no common edges with their neighbors. This is usually the case resulting from the local geometric reconstruction of the manifolds through point cloud. Therefore the DG methods in the literature can not be applied directly. In this regard, we need to write down a more general computational formula. To do so, we pull back all the calculations onto the parametric domain Ω_h . Then we have the following DG form for general problems on manifolds:

$$\begin{aligned} \mathcal{A}_h^{k,l}(u_h, v_h) := & \sum_j \int_{\Omega_h^j} ((\nabla \bar{u}_h)^\top (g_h^k)^{-1} \nabla \bar{v}_h + \bar{u}_h \bar{v}_h) \sqrt{|g_h^k|} dA + \frac{\beta}{h} \sum_{e_h \in \mathcal{E}_h} \int_{e_h} [\bar{u}_h][\bar{v}_h] \{l_{g_h^k}\} dE \\ & - \sum_{e_h \in \bar{\mathcal{E}}_h} \int_{e_h} \{(\nabla \bar{u}_h)^\top (g_h^k)^{-1} (\partial \pi_h^k)^\top n_h\} [\bar{v}_h l_{g_h^k}^+] + \{(\nabla \bar{v}_h)^\top (g_h^k)^{-1} (\partial \pi_h^k)^\top n_h\} [\bar{u}_h l_{g_h^k}^-] dE. \end{aligned} \quad (3.6)$$

Note that in the parametric domain, e_h between two neighbored triangles are unique, which is similar to the standard DG methods. However, different metrics apply to the common edge. This has been reflected in the bilinear form (3.6) where $l_{g_h^k}^+$ and $l_{g_h^k}^-$ might be different.

In order to have a comparison with the DG bilinear form on the exact manifolds, we also consider the following parametric presentation for Γ :

$$\begin{aligned} \mathcal{A}_h^l(u_h, v_h) &:= \sum_j \int_{\Omega_h^j} ((\nabla \bar{u}_h)^\top g^{-1} \nabla \bar{v}_h + \bar{u}_h \bar{v}_h) \sqrt{|g|} dA + \frac{\beta}{h} \sum_{e_h \in \mathcal{E}_h} \int_{e_h} [\bar{u}_h][\bar{v}_h] l_g dE \\ &\quad - \sum_{e_h \in \mathcal{E}_h} \int_{e_h} (\{(\nabla \bar{u}_h)^\top g^{-1} (\partial \pi)^\top n\} [\bar{v}_h] + \{(\nabla \bar{v}_h)^\top g^{-1} (\partial \pi)^\top n\} [\bar{u}_h]) l_g dE. \end{aligned} \quad (3.7)$$

In the following, we denote $\beta_h := \frac{\beta}{h}$. Note that the difference between (3.7) and (3.6) is that the edge metric scaling l_g is the same on every shared edge while $l_{g_h^k}$ in general might be not coincide. In that case the formula in (3.7) is just a rewriting of the formula in (3.5) by replacing the metric tensor g with g_h^k .

3.2 Function spaces associated to DG methods

In order to conduct error analysis for the DG method formulated in (3.6), we introduce necessary function spaces and also their associated norms. They both involve the geometry by $\hat{\Gamma}_h^k$ and Γ_h , the reconstructed piecewise polynomial patches from point cloud and the triangulated original manifold, respectively. Note that Γ_h is just a partition of Γ by curved triangles of diameter h . It is common to consider piecewise Sobolev spaces for DG methods. In particular, we use the notation H_b^r to denote the broken Sobolev spaces

$$H_b^r(\hat{\Gamma}_h^k) := \left\{ v : \hat{\Gamma}_h^k \rightarrow \mathbb{R}, \text{ and } v|_{\hat{\Gamma}_h^{k,j}} \in H^r(\hat{\Gamma}_h^{k,j}), \text{ for all } j \in J \right\}, \quad (3.8)$$

where H^r denotes the standard Sobolev space, and r is the order of the differentiation. The definition in (3.8) can similarly apply to Γ by considering each of the corresponding curved triangles Γ_h^j . The finite element function space of DG method is given in an isoparametric way through parameter domain Ω_h . Precisely we consider piecewise polynomial functions on every parametric triangle patch Ω_h^j , which are then pulled back to the corresponding surface patches:

$$\hat{S}_h^{k,l} := \left\{ v \in L^2(\hat{\Gamma}_h^k) : v|_{\hat{\Gamma}_h^{k,j}} = \bar{v} \circ (\pi_h^k)^{-1} \text{ where } \bar{v} \in P^l(\Omega_h^j) \text{ for all } j \in J \right\}, \quad (3.9)$$

where l is the polynomial order for function values, and k is the polynomial order for reconstructing the local patches from point cloud. Again this types of spaces can also constructed for the exact manifold Γ_h , in which case, we denote by

$$S_h^l := \left\{ v \in L^2(\Gamma_h) : v|_{\Gamma_h^j} = \bar{v} \circ (\pi)^{-1} \text{ where } \bar{v} \in P^l(\Omega_h^j) \text{ for all } j \in J \right\}. \quad (3.10)$$

It is not hard to see that $\hat{S}_h^{k,l} \subset H_b^l(\hat{\Gamma}_h^k)$ and $S_h^l \subset H_b^l(\Gamma_h)$, respectively. We introduce the following spaces

$$V_h^l := H^l(\Gamma_h) + H_b^l(\Gamma_h) \quad \text{and} \quad V_h^{k,l} := H^l(\hat{\Gamma}_h^k) + H_b^l(\hat{\Gamma}_h^k).$$

Their norms can characterize the DG spaces, which is often called DG norms. Here we write down the one for the former

$$\|v_h\|_{V_h^l}^2 = \sum_j \|v_h\|_{H^l(\Gamma_h^j)}^2 + \sum_{e_h \in \mathcal{E}_h} \beta_h \| [v_h] \|_{L^2(e_h)}^2 \quad \text{for every } v_h \in V_h^l.$$

The one for the latter is similar and thus omitted. For simplicity, we also denote

$$\|v_h\|_*^2 = \sum_{e_h \in \mathcal{E}_h} \beta_h \| [v_h] \|_{L^2(e_h)}^2. \quad (3.11)$$

To compare functions defined on Γ_h and $\hat{\Gamma}_h^k$, we rely on the pullback and pushforward operations, which are precisely defined as follows:

$$T_h^k u_h := u_h \circ \pi_h^k \circ (\pi)^{-1}. \quad (3.12)$$

Note the pullback T_h^k is a bijection and both itself and its inverse the pushforward $(T_h^k)^{-1}$ are bounded operators in the sense that:

Lemma 3.1. Let T_h^k and its inverse $(T_h^k)^{-1}$ be defined as (3.12), then

$$\|T_h^k u_h\|_{H^m(\Gamma_h)} \simeq \|u_h\|_{H^m(\hat{\Gamma}_h^k)} \quad \text{for all } 0 \leq m \leq l+1. \quad (3.13)$$

By $a \simeq b$ we mean that there exist positive constants C_1 and C_2 such that $a \leq C_1 b$ and $b \leq C_2 a$.

3.3 Error analysis for Laplace-Beltrami equation

To develop the convergence analysis, we follow the general strategy in [5, 14], but mostly emphasize the geometric error analysis part. It shows that the geometric error are exactly caused by the approximation of the metric tensor. We shall refer to a few lemmas from [5] on DG methods.

Lemma 3.2 (DG trace inequality). For every $e_h^j \in \partial\Gamma_h^j$, and for sufficiently small h , we have

$$\|v_h\|_{L^2(e_h^j)}^2 \leq Ch^{-1} \|v_h\|_{L^2(\Gamma_h^j)}^2 \quad \text{and} \quad \|\nabla_g v_h\|_{L^2(e_h^j)}^2 \leq Ch^{-1} \|\nabla_g v_h\|_{L^2(\Gamma_h^j)}^2. \quad (3.14)$$

Lemma 3.3 (Boundedness and coercivity of DG bilinear form). The DG bilinear form \mathcal{A}_h^l defined on Γ_h is bounded and coercive in DG norm provided that the stabilization parameter β is large enough, i.e.,

$$\mathcal{A}_h^l(u_h, v_h) \leq \|u_h\|_{V_h^l} \|v_h\|_{V_h^l} \quad \text{and} \quad \mathcal{A}_h^l(u_h, u_h) \geq C \|u_h\|_{V_h^l}^2 \quad (3.15)$$

With the above preparation, we are now ready to present our main result on the error bounds of the IPDG method.

Theorem 3.4. Let $u_h^{k,l} \in \hat{S}_h^{k,l}$ be the solution by DG discretization of (3.2), and $u \in H^{l+1}(\Gamma_h)$ is the solution of (3.1). Then we have the following quantitative convergence result:

$$\left\| \hat{u}_h^{k,l} - u \right\|_{L^2(\Gamma_h)} + h \left\| \hat{u}_h^{k,l} - u \right\|_{V_h^l} \leq Ch^{\min\{k,l\}+1} (\|f\|_{L^2(\Gamma_h)} + \|u\|_{H^{l+1}(\Gamma_h)}), \quad (3.16)$$

where $\hat{u}_h^{k,l} = T_h^k u_h^{k,l}$ is the pullback of the function $u_h^{k,l}$ from $\hat{\Gamma}_h^k$ to Γ_h .

Proof. We sketch some of the major steps for a proof strategy, while highlight the part which is different to the one in [5]. We first show the estimate on the DG norm of the error $\left\| \hat{u}_h^{k,l} - u \right\|_{V_h^l}$.

After that we proceed with the $L^2(\Gamma_h)$ norm error estimate.

Step 1: Using triangle inequality, this can be decomposed into:

$$\left\| \hat{u}_h^{k,l} - u \right\|_{V_h^l} \leq \left\| I_h^l u - u \right\|_{V_h^l} + \left\| I_h^l u - \hat{u}_h^{k,l} \right\|_{V_h^l}. \quad (3.17)$$

Step 2: The first term on the right hand side of (3.17) can be estimated using interpolation error estimate and the trace inequality(3.14). This gives

$$\left\| I_h^l u - u \right\|_{V_h^l} \leq Ch^l \|u\|_{H^{l+1}(\Gamma_h)}.$$

Be careful here we have interpolation both on the triangle faces and also on the edges.

Step 3: The second term on the right hand side of (3.17) needs a bit more work. Using the stability estimate in Lemma 3.3

$$\left\| I_h^l u - \hat{u}_h^{k,l} \right\|_{V_h^l}^2 \leq C \mathcal{A}_h^l(I_h^l u - \hat{u}_h^{k,l}, I_h^l u - \hat{u}_h^{k,l}),$$

where $\mathcal{A}(\cdot, \cdot)$ is the bilinear forms induced by the DG discretization of the weak formulation of the PDEs, e.g., Laplace-Beltrami problem. Note that this is formulated on the underlying exact manifold Γ_h .

Step 4: The key point of the proof is to estimate $\mathcal{A}_h^l(I_h^l u - \hat{u}_h^{k,l}, I_h^l u - \hat{u}_h^{k,l})$. Recall

$$\mathcal{A}_h^l(I_h^l u - \hat{u}_h^{k,l}, I_h^l u - \hat{u}_h^{k,l}) \leq \mathcal{A}_h^l(I_h^l u - u, I_h^l u - \hat{u}_h^{k,l}) + \mathcal{A}_h^l(u - \hat{u}_h^{k,l}, I_h^l u - \hat{u}_h^{k,l}). \quad (3.18)$$

The first term of the right hand side can be bounded by interpolation estimate and Lemma 3.3:

$$\mathcal{A}_h^l(I_h^l u - u, v_h) \leq Ch^l \|u\|_{H^{l+1}(\Gamma_h)} \|v_h\|_{V_h^l}, \quad (3.19)$$

for $v_h \in S_h^l$. The second term on the right-hand side of (3.18) looks like a Galerkin orthogonality residual in conformal FEM. In order to analyze it, we consider the weak formulation and the DG approximation of the Laplace-Beltrami equation, which consists of

$$\mathcal{A}_h^l(u, v_h) = \sum_j \int_{\Gamma_h^j} f v_h dA_g$$

and

$$\mathcal{A}_h^{k,l}(u_h^{k,l}, (T_h^k)^{-1} v_h) = \sum_j \int_{\hat{\Gamma}_h^{k,j}} (T_h^k)^{-1} f (T_h^k)^{-1} v_h dA_{g_h^k},$$

where $\mathcal{A}_h^l(\cdot, \cdot)$ and $\mathcal{A}_h^{k,l}(\cdot, \cdot)$ denotes the DG bilinear forms on Γ_h and $\hat{\Gamma}_h^k$, respectively. Their precise forms have been given in (3.7) and (3.6).

Note that

$$\sum_j \int_{\hat{\Gamma}_h^{k,j}} (T_h^k)^{-1} f (T_h^k)^{-1} v_h dA_{g_h^k} = \sum_j \int_{\Gamma_h^j} f v_h \sigma_A dA_g,$$

where $\sigma_A = \frac{dA_{g_h^k}}{dA_g} = \frac{\sqrt{|g_h^k|}}{\sqrt{|g|}}$. This shows

$$\mathcal{A}_h^l(u, v_h) - \mathcal{A}_h^{k,l}(u_h^{k,l}, (T_h^k)^{-1} v_h) = \sum_j \int_{\Gamma_h^j} f v_h (1 - \sigma_A) dA_g.$$

Now we consider to calculate the quantities on the parametric domain Ω_h

$$\begin{aligned} & \mathcal{A}_h^l(T_h^k u_h^{k,l}, v_h) \\ &= \sum_j \int_{\Omega_h^j} (\nabla \bar{u}_h^{k,l})^\top g^{-1} \nabla \bar{v}_h \sqrt{|g|} dA + \beta_h \sum_{\bar{e}_h \in \bar{\mathcal{E}}_h} \int_{\bar{e}_h} [\bar{u}_h^{k,l}] [\bar{v}_h] l_g dE \\ & \quad - \sum_{\bar{e}_h \in \bar{\mathcal{E}}_h} \int_{\bar{e}_h} \left(\{ (\nabla \bar{u}_h^{k,l})^\top g^{-1} \partial \pi^\top n \} [\bar{v}_h] + \{ (\nabla \bar{v}_h)^\top g^{-1} \partial \pi^\top n \} [\bar{u}_h^{k,l}] \right) l_g dE \end{aligned}$$

while

$$\begin{aligned} & \mathcal{A}_h^{k,l}(u_h^{k,l}, (T_h^k)^{-1} v_h) \\ &= \sum_j \int_{\Omega_h^j} (\nabla \bar{u}_h^{k,l})^\top (g_h^k)^{-1} \nabla \bar{v}_h \sqrt{|g_h^k|} dA + \beta_h \sum_{\bar{e}_h \in \bar{\mathcal{E}}_h} \int_{\bar{e}_h} [\bar{u}_h^{k,l}] [\bar{v}_h] \{ l_{g_h^k} \} dE - \\ & \quad \sum_{\bar{e}_h \in \bar{\mathcal{E}}_h} \int_{\bar{e}_h} \{ (\nabla \bar{u}_h^{k,l})^\top (g_h^k)^{-1} (\partial \pi_h^k)^\top n_h \} [\bar{v}_h l_{g_h^k}] + \{ (\nabla \bar{v}_h)^\top (g_h^k)^{-1} (\partial \pi_h^k)^\top n_h \} [\bar{u}_h^{k,l} l_{g_h^k}] dE. \end{aligned}$$

We define

$$\mathcal{R}(v_h) := \mathcal{A}_h^l(u - \hat{u}_h^{k,l}, v_h). \quad (3.20)$$

which is similar but different to the Galerkin orthogonality term. We have that

$$\begin{aligned} \mathcal{R}(v_h) &= \mathcal{A}_h^{k,l}(u_h^{k,l}, (T_h^k)^{-1} v_h) - \mathcal{A}_h^l(T_h^k u_h^{k,l}, v_h) + \mathcal{A}_h^l(u, v_h) - \mathcal{A}_h^{k,l}(u_h^{k,l}, (T_h^k)^{-1} v_h) \\ &= \mathcal{A}_h^{k,l}(u_h^{k,l}, (T_h^k)^{-1} v_h) - \mathcal{A}_h^l(T_h^k u_h^{k,l}, v_h) + \sum_j \int_{\Gamma_h^j} f v_h (1 - \sigma_A) dA_g, \end{aligned}$$

which leads to

$$\begin{aligned}
\mathcal{R}(v_h) = & \sum_j \int_{\Omega_h^j} (\nabla \bar{u}_h^{k,l})^\top ((g_h^k)^{-1} - g^{-1}) \nabla \bar{v}_h \sqrt{|g_h^k|} + (\nabla \bar{u}_h^{k,l})^\top g^{-1} \nabla \bar{v}_h \left(\sqrt{|g_h^k|} - \sqrt{|g|} \right) dA \\
& - \sum_{\bar{e}_h \in \bar{\mathcal{E}}_h} \int_{\bar{e}_h} \{ (\nabla \bar{u}_h^{k,l})^\top ((g_h^k)^{-1} (\partial \pi_h^k)^\top n_h - g^{-1} (\partial \pi)^\top n) \} [\bar{v}_h l_{g_h^k}] dE \\
& - \sum_{\bar{e}_h \in \bar{\mathcal{E}}_h} \int_{\bar{e}_h} \{ (\nabla \bar{v}_h)^\top ((g_h^k)^{-1} (\partial \pi_h^k)^\top n_h - g^{-1} (\partial \pi)^\top n) \} [\bar{u}_h^{k,l} l_{g_h^k}] dE \\
& - \sum_{\bar{e}_h \in \bar{\mathcal{E}}_h} \int_{\bar{e}_h} \{ (\nabla \bar{u}_h^{k,l})^\top g^{-1} (\partial \pi)^\top n \} [\bar{v}_h (l_{g_h^k} - l_g)] dE \\
& - \sum_{\bar{e}_h \in \bar{\mathcal{E}}_h} \int_{\bar{e}_h} \{ (\nabla \bar{v}_h)^\top g^{-1} (\partial \pi)^\top n \} [\bar{u}_h^{k,l} (l_{g_h^k} - l_g)] dE \\
& + \beta_h \sum_{\bar{e}_h \in \bar{\mathcal{E}}_h} \int_{\bar{e}_h} [\bar{u}_h^{k,l}] [\bar{v}_h] \{ (l_{g_h^k} - l_g) \} dE + \int_{\Omega_h^j} \bar{f} \bar{v}_h \left(\sqrt{|g|} - \sqrt{|g_h^k|} \right) dA.
\end{aligned} \tag{3.21}$$

Taking into account the geometric error estimates in Theorem 2.9, each of the terms on the right-hand side of (3.21) can be estimated. The details of these estimates are given in Appendix B. To summarize all the estimates there, we derive that

$$\mathcal{R}(v_h) \leq C_1 h^{k+1} \left\| T_h^k u_h^{k,l} \right\|_{V_h^l} \|v_h\|_{V_h^l} + C_2 h^{k+1} \|f\|_{L^2(\Gamma_h)} \|v_h\|_{L^2(\Gamma_h)}, \tag{3.22}$$

where $\left\| T_h^k u_h^{k,l} \right\|_{V_h^l}$ is uniformly bounded independent of h . Then we go back to (3.18) with (3.19) $m = l + 1$ and (3.22) to have the statement. In order to estimate $\left\| \hat{u}_h^{k,l} - u \right\|_{L^2(\Gamma_h)}$, we leverage the following dual problem of (3.1):

$$-\Delta_g z + z = \hat{u}_h^{k,l} - u \quad \text{for } z \in H^2(\Gamma_h) \quad \text{and} \quad \|z\|_{H^2(\Gamma_h)} \leq C \left\| \hat{u}_h^{k,l} - u \right\|_{L^2(\Gamma_h)}. \tag{3.23}$$

Testing with $\hat{u}_h^{k,l} - u$ on both sides gives us that

$$\left\| \hat{u}_h^{k,l} - u \right\|_{L^2(\Gamma_h)}^2 = \mathcal{A}_h^l(z, \hat{u}_h^{k,l} - u) = \mathcal{A}_h^l(\hat{u}_h^{k,l} - u, z - I_h^l z) + \mathcal{A}_h^l(\hat{u}_h^{k,l} - u, I_h^l z).$$

Then, applying standard boundedness estimate in Lemma 3.3 to the first term on the right-hand side, we have

$$\mathcal{A}_h^l(\hat{u}_h^{k,l} - u, z - I_h^l z) \leq \left\| \hat{u}_h^{k,l} - u \right\|_{V_h^l} \|z - I_h^l z\|_{V_h^l} \leq Ch^{k+1} \|u\|_{H^{k+1}(\Gamma_h)} \|z\|_{H^2(\Gamma_h)}.$$

For the second term, we use the estimate from (3.22),

$$\begin{aligned}
& \mathcal{A}_h^l(\hat{u}_h^{k,l} - u, I_h^l z) = \mathcal{R}(I_h^l z) \\
& \leq C_1 h^{k+1} \left\| T_h^k u_h^{k,l} \right\|_{V_h^l} \|I_h^l z\|_{V_h^l} + C_2 h^{k+1} \|f\|_{L^2(\Gamma)} \|I_h^l z\|_{L^2(\Gamma_h)} \\
& \leq C \left(C_1 h^{k+1} \left\| T_h^k u_h^{k,l} \right\|_{V_h^l} + C_2 h^{k+1} \|f\|_{L^2(\Gamma)} \right) \|z\|_{H^2(\Gamma_h)}
\end{aligned}$$

Combining with (3.23), we end up with the expected estimates in (3.16) for the L^2 norm. This concludes the proof in combination with the DG norm estimates. \square

3.4 Error analysis for the eigenvalue problem

Let the eigenpair (λ, u) be the solution of the eigenvalue problem (3.3), or equivalently (3.4). The DG discretization of eigenvalue problem (3.3) can be formulated as finding pairs $(\lambda_h^{k,l}, u_h^{k,l}) \in$

$(\mathbb{R}, V_h^{k,l})$ such that

$$\mathcal{A}_h^{k,l}(u_h^{k,l}, v_h) = (\lambda_h^{k,l} + 1) \sum_j \int_{\Omega_h^j} \bar{u}_h^{k,l} \bar{v}_h \sqrt{|g_h^k|} dA, \quad \text{for all } v_h \in V_h^{k,l}. \quad (3.24)$$

Similarly, the discrete eigenvalues of discrete problem (3.24) can be ordered as $0 = \lambda_{h,1}^{k,l} < \lambda_{h,2}^{k,l} \leq \dots \leq \lambda_{h,N}^{k,l}$, and the corresponding eigenfunctions $u_{h,i}^{k,l}$ ($i = 1, \dots, N$) can be normalized as $(u_{h,i}^{k,l}, u_{h,j}^{k,l}) = \delta_{ij}$ where N is the dimension of the DG function space.

Let $G : L^2(\Gamma_h) \rightarrow H^1(\Gamma_h) \subset L^2(\Gamma_h)$ be the solution operator of the Laplace-Beltrami problem (3.2) which is defined as

$$\mathcal{A}(Gf, v) = (f, v), \quad \forall v \in H^1(\Gamma) \quad (3.25)$$

and $G_h^{k,l} : L^2(\hat{\Gamma}_h^k) \rightarrow V_h^{k,l} \subset L^2(\hat{\Gamma}_h^k)$ be the discrete solution operator which is defined as

$$\mathcal{A}_h^{k,l}(G_h^{k,l} f, v_h) = ((T_h^k)^{-1} f, v_h), \quad \forall v_h \in V_h^{k,l}. \quad (3.26)$$

Both G and $G_h^{k,l}$ are self-adjoint. Let μ (or $\mu_h^{k,l}$) be the eigenvalue of G (or $G_h^{k,l}$). Then, we can relate the eigenvalue of (3.3) and the eigenvalue of the operator G by $\mu = \frac{1}{1+\lambda}$. Similarly, we have $\mu^{k,l} = \frac{1}{1+\lambda_h^{k,l}}$. In addition, we have

$$\lambda_h^{k,l} - \lambda = (1 + \lambda_h^{k,l})(1 + \lambda)(\mu_i - \mu_h^{k,l}). \quad (3.27)$$

The following lemma tells that the eigenvalues are invariant under geometric transformation operator T_h^k and its inverse $(T_h^k)^{-1}$.

Lemma 3.5. *If $G\hat{v} = \mu\hat{v}$, then $(T_h^k)^{-1}G\hat{v} = \mu(T_h^k)^{-1}\hat{v}$. Similarly, if $G_h^k v_h = \mu_h^k v_h$, then $T_h^k G_h^k v_h = \mu_h^k T_h^k v_h$.*

Proof. This is shown using the fact that the operators $(T_h^k)^\pm$ and the scalar multiplication are commutable, i.e., $\mu_h^k T_h^k v_h = T_h^k \mu_h^k v_h$ and $\mu(T_h^k)^{-1}\hat{v} = (T_h^k)^{-1}\mu\hat{v}$. \square

Using the above lemma, we have the following result.

Lemma 3.6. *Let $\mu_h^{k,l}$ be an eigenvalue of the operator $G_h^{k,l}$ on $\hat{\Gamma}_h^k$ with eigenfunction $u_h^{k,l}$. Define an solution operator*

$$\tilde{G}_h^{k,l} := T_h^k G_h^{k,l} (T_h^k)^{-1} \quad \text{on } \Gamma_h. \quad (3.28)$$

Then $\mu_h^{k,l}$ is an eigenvalue of $\tilde{G}_h^{k,l}$ and the corresponding eigenfunction is $T_h^k u_h^{k,l}$.

Proof. Let $\hat{u}_h^{k,l} := T_h^k u_h^{k,l}$. Notice that $G_h^{k,l} u_h^{k,l} = \mu_h^{k,l} u_h^{k,l}$ which implies that $G_h^{k,l} (T_h^k)^{-1} \hat{u}_h^{k,l} = \mu_h^{k,l} (T_h^k)^{-1} \hat{u}_h^{k,l} = (T_h^k)^{-1} \mu_h^{k,l} \hat{u}_h^{k,l}$. It tells that $T_h^k G_h^{k,l} (T_h^k)^{-1} \hat{u}_h^{k,l} = \mu_h^{k,l} \hat{u}_h^{k,l}$, which completes the proof. \square

To simplify the notation, we define

$$\mathcal{E}_h^{k,l}(G) := G - \tilde{G}_h^{k,l}. \quad (3.29)$$

Using Theorem 3.4 for the source problem, we can show the operator approximation result

Lemma 3.7. *Let $\tilde{G}_h^{k,l} : L^2(\Gamma_h) \rightarrow V_h^l \subset L^2(\Gamma_h)$ be defined as in (3.28), and $\mathcal{E}_h^{k,l}(G)$ be given as (3.29). Then the following approximation properties hold:*

$$\left\| \mathcal{E}_h^{k,l}(G) \right\|_{\mathcal{L}(L^2(\Gamma_h))} = \mathcal{O}(h^{\min\{k,l\}+1}). \quad (3.30)$$

In particular, we have

$$\lim_{h \rightarrow 0} \left\| \mathcal{E}_h^{k,l}(G) \right\|_{\mathcal{L}(L^2(\Gamma_h))} \rightarrow 0. \quad (3.31)$$

Let $\rho(G)$ (or $\rho(\tilde{G}_h^{k,l})$) denote the resolvent set of operator G (or $\tilde{G}_h^{k,l}$), and $\sigma(G)$ (or $\sigma(\tilde{G}_h^{k,l})$) denote the spectrum set of operator G (or $\tilde{G}_h^{k,l}$). We define the spectral projection operator

$$E(\mu) := \frac{1}{2\pi i} \int_\gamma (z - G)^{-1} dz.$$

Here $\gamma \subset \rho(G)$ is a curve in the complex domain which encloses $\mu \in \sigma(G)$ but no other eigenvalues of G . Let $R(E)$ denote the range of E . Let μ be an eigenvalue of the operator G , and it has algebraic multiplicity m . Then, combining Theorem 9.1 in [9] and (3.31) implies that no pollution of the spectrum, i.e. γ encloses exactly m discrete eigenvalues $\left\{ \mu_{h,i}^{k,l} \right\}_{i=1}^m$ of $\tilde{G}_h^{k,l}$ approximating μ .

Using the Babuška-Osborn spectral approximation theory [8], we have the following convergence results on eigenvalues and eigenfunctions.

Theorem 3.8. *Let $\mu_h^{k,l}$ be an eigenvalue converging to μ . Let $\hat{u}_h^{k,l}$ be a unit eigenfunction of $\tilde{G}_h^{k,l}$ associated with the eigenvalue $\mu_h^{k,l}$. Then there exists a unit eigenvector $u \in R(E)$ such that the following estimates hold*

$$\|u - \hat{u}_h^{k,l}\|_{L^2(\Gamma_h)} \leq Ch^{\min\{k,l\}+1}, \quad (3.32)$$

$$|\mu - \mu_h^{k,l}| \leq C(\lambda)(h^{\min\{k+1,2l\}}), \quad (3.33)$$

$$|\lambda - \lambda_h^{k,l}| \leq C(\lambda)(h^{\min\{k+1,2l\}}), \quad (3.34)$$

where $l \geq 1$ and $k \geq 1$ are orders of the local polynomials for function and geometry approximations, respectively.

Proof. For the eigenfunction approximation, Theorem 7.4 in [8] and the approximation property (3.30) already imply that

$$\|u - \hat{u}_h^{k,l}\|_{L^2(\Gamma_h)} \leq \|\mathcal{E}_h^{k,l}(G)|_{R(E)}\|_{L^2(\Gamma_h)} \leq Ch^{\min\{k,l\}+1}. \quad (3.35)$$

To establish the eigenvalue approximation result (3.33), we apply Theorem 7.3 in [8]. Let v_1, \dots, v_m be any orthonormal basis for $R(E)$. Then, Theorem 7.3 in [8] implies that there exists a constant C such that

$$|\mu - \mu_h| \leq C \sum_{j,k=1}^m |(\mathcal{E}_h^{k,l}(G)v_j, v_k)| + C\|\mathcal{E}_h^{k,l}(G)|_{R(E)}\|_{L^2(\Gamma_h)}^2. \quad (3.36)$$

The second term can be bounded by $\mathcal{O}(h^{2\min\{k,l\}+2})$. For the first term, we have

$$\begin{aligned} & \left(\mathcal{E}_h^{k,l}(G)v_j, v_k \right) \\ &= \mathcal{A}(Gv_j, Gv_k) - \mathcal{A}_h^l(\tilde{G}_h^{k,l}v_j, \tilde{G}_h^{k,l}v_k) + \mathcal{A}_h^l(\tilde{G}_h^{k,l}v_j, \tilde{G}_h^{k,l}v_k) - \left(\tilde{G}_h^{k,l}v_j, v_k \right). \end{aligned} \quad (3.37)$$

Now we estimate each of the two paired terms on the right hand side of (3.37) individually. The first one gives

$$\begin{aligned} & \mathcal{A}(Gv_j, Gv_k) - \mathcal{A}_h^l(\tilde{G}_h^{k,l}v_j, \tilde{G}_h^{k,l}v_k) = \mathcal{A}_h^l(Gv_j, Gv_k) - \mathcal{A}_h^l(\tilde{G}_h^{k,l}v_j, \tilde{G}_h^{k,l}v_k) \\ &= \mathcal{A}_h^l(Gv_j - \tilde{G}_h^{k,l}v_j, Gv_k) + \mathcal{A}_h^l(\tilde{G}_h^{k,l}v_j, Gv_k - \tilde{G}_h^{k,l}v_k) \\ &= \mathcal{A}_h^l(\mathcal{E}_h^{k,l}(G)v_j, \tilde{G}_h^{k,l}v_k) + \mathcal{A}_h^l(\tilde{G}_h^{k,l}v_j, \mathcal{E}_h^{k,l}(G)v_k) + \mathcal{A}_h^l(\mathcal{E}_h^{k,l}(G)v_j, \mathcal{E}_h^{k,l}(G)v_k), \end{aligned} \quad (3.38)$$

where the first equality holds since $Gv_j, Gv_k \in H^2(\Gamma_h)$ are continuous for two dimensional Γ_h . Notice that the third term on the last line of (3.38) can be easily estimated by

$$\mathcal{A}_h^l(\mathcal{E}_h^{k,l}(G)v_j, \mathcal{E}_h^{k,l}(G)v_k) \leq \left\| \mathcal{E}_h^{k,l}(G)v_j \right\|_{V_h^l} \left\| \mathcal{E}_h^{k,l}(G)v_k \right\|_{V_h^l}.$$

While for the first and the second terms on last line of (3.38), we recall to (3.20), which then indicates the following

$$\mathcal{A}_h^l(\mathcal{E}_h^{k,l}(G)v_j, \tilde{G}_h^{k,l}v_k) + \mathcal{A}_h^l(\tilde{G}_h^{k,l}v_j, \mathcal{E}_h^{k,l}(G)v_k) \leq \mathcal{R}(\tilde{G}_h^{k,l}v_k) + \mathcal{R}(\tilde{G}_h^{k,l}v_j) \leq Ch^{k+1},$$

where $\mathcal{R}(\cdot)$ is defined in (3.20) and estimated in (3.22).

For the second term on the right hand side of (3.37), we have

$$\begin{aligned}
& |\mathcal{A}_h^l(\tilde{G}_h^{k,l}u, \tilde{G}_h^{k,l}v) - (\tilde{G}_h^{k,l}u, v)| \\
\leq & |\mathcal{A}_h^l(\tilde{G}_h^{k,l}u, \tilde{G}_h^{k,l}v) - \mathcal{A}_h^{k,l}(G_h^{k,l}T_h^k u, G_h^{k,l}T_h^k v) + \mathcal{A}_h^{k,l}(G_h^{k,l}T_h^k u, G_h^{k,l}T_h^k v) - (G_h^{k,l}T_h^k u, T_h^k v)| \\
& + |(G_h^{k,l}T_h^k u, T_h^k v) - (\tilde{G}_h^{k,l}u, v)| \\
\leq & Ch^{k+1} + \underbrace{|\mathcal{A}_h^{k,l}(G_h^{k,l}T_h^k u, G_h^{k,l}T_h^k v) - (G_h^{k,l}T_h^k u, T_h^k v)|}_{=0} + Ch^{k+1},
\end{aligned}$$

where the first and the third terms are due to the geometric error estimates from Theorem 2.9. Summarizing the above estimates, it concludes the proof of (3.32). (3.34) is a direct consequence of (3.33) and (3.27). \square

Remark 3.9. Note that the conclusion of Theorem 3.8 and its proof can also be applied to the continuous Galerkin method on surfaces. We notice here that the geometric approximation error and the function discretization error are not of the same order in the higher-order element cases for the eigenvalue approximation, i.e., the convergence rates of order $\mathcal{O}(h^{\min\{2l, 2k\}})$, which was observed in some numerical cases in [11]. The proven error estimates turn out to be theoretically sharp given the geometric approximation error and the function approximation error there. To see this, we consider an example on unit sphere Γ . Let the approximation manifold be another sphere $\hat{\Gamma}_h^k$ with radius $1 + h^{k+1}$, which satisfies the geometric approximation error $\|\pi - \pi_h^k\| \leq h^{k+1}$. Now we consider the Laplace-Beltrami operator on Γ_h^k and its eigenvalues. Using the analytical formula of sphere harmonics, we know that the eigenvalues associated to $\hat{\Gamma}_h^k$ are of the following form $\lambda_h^k \in \left(\frac{n(n+1)}{(1+h^{k+1})}\right)_{n=1}^{\infty}$, while for Γ are $\lambda \in (n(n+1))_{n=1}^{\infty}$. The error of eigenvalue approximation is $|\lambda - \lambda_h^k| = \frac{n(n+1)h^{k+1}}{(1+h^{k+1})}$. This shows even in this ideal case, the eigenvalues' approximation errors of order h^{2k} can not be achieved, when the geometric approximation error is of order $\mathcal{O}(h^{k+1})$ for $k > 1$. This serves as an example to justify our results.

4 Numerical results

In the following, we present a series of benchmark numerical experiments to verify our theoretical findings on the error analysis of the proposed DG method on point clouds. We pick two representative manifolds, the unit sphere and a torus surface, which have genus zero and one, respectively. Before going to numerical results of the optimal convergence rates of the DG method for solving both source and eigenvalue problems of LB operator on point clouds, we first provide a validation of the geometric error bounds of Algorithm 1.

4.1 Geometric error

To simplify the presentation, we introduce the following notations

$$e_n^k = \max_{i \in N} |\psi^i - \xi^i|, \quad \text{and} \quad e_t^k = \max_{i \in N} |\psi_{\Omega_h}^i - \xi_{\Omega_h}^i|,$$

where the superscript k denotes the k th order polynomials used in the patch reconstruction from point cloud, and N represents the number of nodal points of Ω_h .

We first check the accuracy claimed for Algorithm 1 based on point cloud which is sampled from the unit sphere and is uniform distributed on its spherical coordinate. In the first test, the initial mesh is generated using CGAL [3] whose vertices are $\mathcal{O}(h^2)$ to the unit sphere. In practice, such meshes can be generated using Poisson surface reconstruction [26] which is available in the computational geometry algorithm library CGAL [3]. To depict the convergence rates, we conduct a uniform refinement for each triangle by dividing it into four similar subtriangles. A main difference between the classical refinement for surface finite element methods [15] is that we do not ask for the precise embedding of submanifolds, e.g., the level set functions or parameterization functions. Note that Assumption 2.4 holds already due to the interpolation of the mesh in this example. For

the general case, we can adjust the vertices of the mesh using the point cloud reconstruction before proceeding with uniform refinements, and this costs no extra work.

To assess the result of Proposition 2.6, we report the difference between the reconstructed nodal points and the exact nodal ones in Table 1. Due to the structure of the sphere, the exact nodal points are obtained by stretching the reconstructed nodes along with radial directions. Note that the error bounds of $\mathcal{O}(h^{k+1})$ can be observed except for outliers. We also list the errors after projecting the paired nodal points onto the parametric domain Ω_h in Table 2, which illustrates the $\mathcal{O}(h^{k+2})$ convergence rate. These ally with the theoretical results established in Proposition 2.6.

Table 1: Errors of patch reconstruction from point cloud on unit sphere

N_v	e_n^1	Order	e_n^2	Order	e_n^3	Order	e_n^4	Order
222	1.12e-02	–	1.52e-05	–	1.35e-05	–	9.02e-08	–
882	2.95e-03	1.94	1.09e-05	0.47	2.68e-06	2.34	4.27e-08	1.09
3522	7.21e-04	2.03	7.14e-07	3.94	9.42e-08	4.84	3.40e-10	6.98
14082	1.80e-04	2.00	4.65e-08	3.94	4.83e-09	4.29	3.56e-12	6.58
56322	4.64e-05	1.96	3.77e-09	3.62	4.07e-10	3.57	1.22e-13	4.87

Table 2: Decomposed error in the parametric domain for sphere point cloud

N_v	e_t^1	Order	e_t^2	Order	e_t^3	Order	e_t^4	Order
222	3.88e-04	–	1.63e-05	–	1.16e-05	–	1.44e-07	–
882	1.71e-03	-2.15	1.81e-05	-0.16	5.19e-06	1.16	1.15e-07	0.33
3522	2.13e-04	3.01	5.92e-07	4.94	1.61e-07	5.01	9.09e-10	6.99
14082	2.69e-05	2.98	1.91e-08	4.96	5.41e-09	4.90	8.15e-12	6.80
56322	3.47e-06	2.96	7.04e-10	4.76	2.37e-10	4.51	9.61e-14	6.41

Notice that, in the sphere case, surprisingly, we can observe some geometric superconvergence phenomenon in the reconstructed patches when the even-order polynomial is employed like quadratic and quartic polynomials. This implies the superconvergence geometric approximation results in the eigenvalue problem later.

Another set of tests are implemented with point cloud presentation of a torus surface:

$$\begin{cases} x = (4 \cos(\theta) + 1) \cos(\phi), \\ y = (4 \cos(\theta) + 1) \sin(\phi), \\ z = 4 \sin(\theta). \end{cases} \quad (4.1)$$

The point cloud is generated from uniformly distributed points in (θ, ϕ) coordinate and then projected onto the torus.

In Table 3, we present the numerical error for the reconstructed nodal points as the first example. We can observe error bounds of order $\mathcal{O}(h)^{k+1}$ when k th order polynomials are used. Similarly, $\mathcal{O}(h^{k+2})$ error bounds for the nodal pairs projected onto the parameter domain coincide with Proposition 2.6. Different from the unit sphere case, there seems no geometrical superconvergence for even polynomials, different to the previous example.

4.2 PDEs on point cloud of the unit sphere

Now we show the numerical results of the proposed DG method for discretizing the Laplace-Beltrami operator on the point cloud generated patches. We first give results for the Laplace-Beltrami equation (3.1). The right hand side function $f(x)$ is chosen to fit the exact solution $u(x) = x_1 x_2$. In this test, we choose the finite element degree l and the geometric degree k equal to some p for $p \in \{1, 2, 3, 4\}$. According to the Theorem 3.4, we would expect $\mathcal{O}(\max\{h^{l+1}, h^{k+1}\})$ for L_2 error and $\mathcal{O}(\max\{h^l, h^k\})$ convergence for H^1 error for sufficiently small h . Without causing confusion, we use e^p (or De^p) to denote the L^2 (or H^1) error with p th order degree. The numerical results are plotted in Figure 2, where optimal convergence rates can be observed as desired.

Then we test with the DG discretizing of the Laplace-Beltrami eigenvalue problem (3.3) using the same surface patches. For the Laplace-Beltrami operator on the unit sphere, eigenvalues and

Table 3: Errors of patch reconstruction from point cloud on torus

N_v	e_n^1	Order	e_n^2	Order	e_n^3	Order	e_n^4	Order
200	4.67e-02	–	1.66e-03	–	3.17e-04	–	6.63e-05	–
800	1.44e-02	1.69	7.79e-04	1.09	8.62e-05	1.88	9.45e-06	2.81
3200	3.39e-03	2.09	5.81e-05	3.75	2.54e-06	5.08	1.98e-07	5.58
12800	9.00e-04	1.91	5.81e-06	3.32	1.15e-07	4.47	3.92e-09	5.66
51200	2.48e-04	1.86	1.09e-06	2.42	7.06e-09	4.02	1.14e-10	5.11

Table 4: Decomposed error in the parametric domain for point cloud on torus

N_v	e_t^1	Order	e_t^2	Order	e_t^3	Order	e_t^4	Order
200	2.92e-03	–	1.37e-03	–	3.48e-04	–	7.41e-05	–
800	1.67e-02	-2.52	1.85e-03	-0.43	2.22e-04	0.65	4.04e-05	0.88
3200	2.46e-03	2.77	1.25e-04	3.89	7.83e-06	4.82	6.07e-07	6.06
12800	3.17e-04	2.95	8.34e-06	3.90	2.46e-07	4.99	1.32e-08	5.53
51200	4.34e-05	2.87	6.82e-07	3.61	8.29e-09	4.89	2.42e-10	5.76

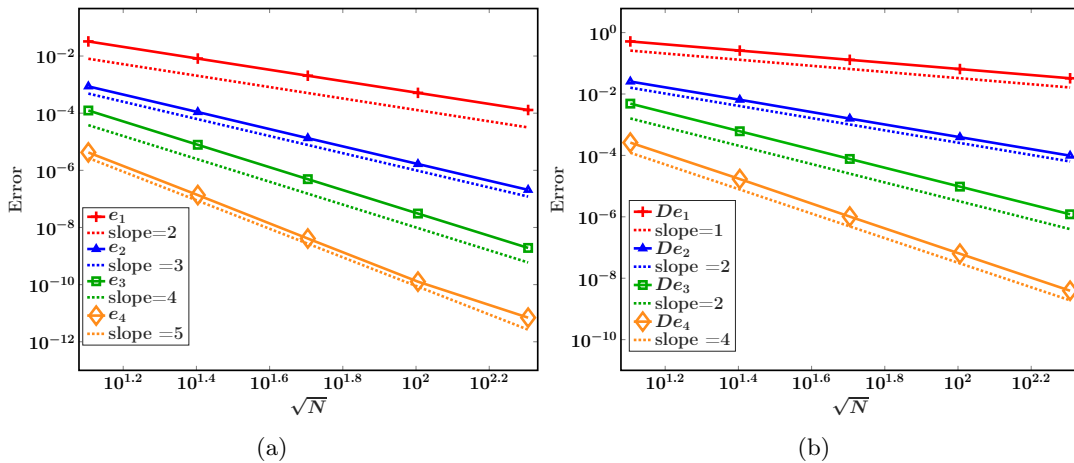


Figure 2: Numerical results of Laplace-Beltrami equation on the unit sphere. (a): L_2 error; (b): H_1 error.

eigenfunctions are known explicitly. In the experiments, we focus on the computation of the first nonzero eigenvalue $\lambda_2 = \lambda_3 = \lambda_4 = 2$. The corresponding eigenfunctions are $u_i = x_{i-1}$ for $i = 2, 3, 4$, which are called spherical harmonics [1].

According to Theorem 3.8, the eigenvalue λ_i converges optimally at the rate of $\mathcal{O}(\max\{h^{2l}, h^{k+1}\})$. Taking $l = 2$ as example, we need $k = 3$ to observe the optimal convergence. The corresponding numerical results are reported in Table 5, where the expected rates can be observed.

We also test for another choice of k and l . The numerical results for $l = 3$ and $k = 4$ are documented in Table 6. According to Theorem 3.8, we would only expect $\mathcal{O}(h^5)$ order convergence in the eigenvalues. However, interestingly, $\mathcal{O}(h^6)$ order convergence is observed for the eigenvalue, which is due to the superconvergence of the geometric approximation reported in the previous section. To further demonstrate this, we test the case $k = l = 2$. The numerical output are reported in Table 7. Again, improved convergence rates are observed, which support the error bounds $\mathcal{O}(\max\{h^{2l}, h^{k+2}\})$ when k is even. Surprisingly, we also observe the $\mathcal{O}(h^{k+2})$ (or $\mathcal{O}(h^{k+1})$) order superconvergence for eigenfunctions' approximation in L^2 norm (or H^1 norm).

4.3 PDEs on point cloud of a torus

In the following, we present numerical solutions of the DG method on the patches reconstructed from the torus point cloud. Similar to the last example, we start with the Laplace-Beltrami equation (3.1). The cooked up exact solution is $u(x) = x_1 - x_2$ and then the right hand side function $f(x)$ can be simply computed. We set $k = l = p$ for some $p = 1, \dots, 4$. The numerical

Table 5: Numerical result of Laplace-Beltrami eigenvalue problem on the unit sphere point cloud when $l = 2$ and $k = 3$

i	N_v	$ \lambda_i - \lambda_{i,h} $	Order	$\ u_i - u_{i,h}\ _{0,\Gamma_h}$	Order	$ u_i - u_{i,h} _{1,\Gamma_h}$	Order
2	222	3.99e-05	–	4.20e-04	–	1.07e-02	–
2	882	2.82e-06	3.84	5.26e-05	3.01	2.72e-03	1.99
2	3522	1.81e-07	3.97	6.59e-06	3.00	6.83e-04	1.99
2	14082	1.16e-08	3.97	8.27e-07	3.00	1.72e-04	1.99
3	222	5.18e-05	–	4.28e-04	–	1.09e-02	–
3	882	3.50e-06	3.91	5.37e-05	3.01	2.76e-03	1.99
3	3522	2.25e-07	3.97	6.74e-06	3.00	6.94e-04	1.99
3	14082	1.43e-08	3.98	8.45e-07	3.00	1.74e-04	1.99
4	222	6.52e-05	–	4.45e-04	–	1.12e-02	–
4	882	4.38e-06	3.92	5.58e-05	3.01	2.85e-03	1.99
4	3522	2.79e-07	3.97	6.98e-06	3.00	7.17e-04	1.99
4	14082	1.77e-08	3.98	8.75e-07	3.00	1.80e-04	1.99

Table 6: Numerical result of Laplace-Beltrami eigenvalue problem on the unit sphere point cloud when $l = 3$ and $k = 4$

i	N_v	$ \lambda_i - \lambda_{i,h} $	Order	$\ u_i - u_{i,h}\ _{0,\Gamma_h}$	Order	$ u_i - u_{i,h} _{1,\Gamma_h}$	Order
2	222	1.46e-08	–	2.00e-05	–	7.08e-04	–
2	882	8.98e-10	4.04	1.33e-06	3.92	9.35e-05	2.93
2	3522	1.59e-11	5.82	8.01e-08	4.06	1.14e-05	3.04
2	14082	1.69e-11	-0.08	4.59e-09	4.13	1.34e-06	3.09
3	222	3.15e-08	–	1.97e-05	–	6.95e-04	–
3	882	1.21e-09	4.72	1.19e-06	4.07	8.52e-05	3.04
3	3522	1.73e-11	6.14	7.84e-08	3.93	1.11e-05	2.94
3	14082	2.10e-11	-0.28	4.72e-09	4.06	1.36e-06	3.03
4	222	4.84e-08	–	1.77e-05	–	6.39e-04	–
4	882	1.48e-09	5.06	1.22e-06	3.87	8.75e-05	2.88
4	3522	1.88e-11	6.31	7.12e-08	4.11	1.04e-05	3.08
4	14082	3.30e-11	-0.82	4.97e-09	3.84	1.41e-06	2.88

errors are documented in Figure 3. From there we can spot the optimal convergence rates for both L^2 and H^1 errors.

For the comparison of eigenvalues for the Laplace-Beltrami operator, it is different to the unit sphere case, as the exact eigenvalues of the Laplace-Beltrami operator on a torus are not known to us. To study the convergence rates, we use the following relative error

$$Err_i = \frac{|\lambda_{i,h_{j+1}} - \lambda_{i,h_j}|}{\lambda_{i,h_{j+1}}}, \quad (4.2)$$

where h_j is the mesh-size on the j th level of meshes. The numerical results are reported in Figure 4a for $k = l = 2$. We compare the first five nontrivial eigenvalues. What stands out in this figure is that 4th order convergence is shown up, which seems indicate $\mathcal{O}(\max\{h^{2l}, h^{k+2}\})$ bounds for eigenvalue approximation when k is even. In Figure 4b, we display the eigenvalue approximation error when $k = l = 4$. Superconvergence of the geometric approximations are presented again in both the even-order polynomial cases. This kind of superconvergence results may deserve further investigation.

Table 7: Numerical result of Laplace-Beltrami eigenvalue problem on the unit sphere when $k = 2$ and $l = 2$

i	N_v	$ \lambda_i - \lambda_{i,h} $	Order	$\ u_i - u_{i,h}\ _{0,\Gamma_h}$	Order	$ u_i - u_{i,h} _{1,\Gamma_h}$	Order
2	222	1.09e-04	–	2.12e-05	–	1.21e-03	–
2	882	7.65e-06	3.86	3.58e-06	2.58	4.83e-04	1.33
2	3522	4.67e-07	4.04	2.16e-07	4.06	6.08e-05	3.00
2	14082	2.92e-08	4.00	1.34e-08	4.01	7.62e-06	3.00
3	222	1.22e-04	–	2.42e-05	–	1.20e-03	–
3	882	8.28e-06	3.90	3.86e-06	2.66	4.90e-04	1.30
3	3522	5.14e-07	4.02	2.35e-07	4.04	6.16e-05	3.00
3	14082	3.22e-08	4.00	1.46e-08	4.00	7.72e-06	3.00
4	222	1.44e-04	–	2.77e-05	–	1.18e-03	–
4	882	9.94e-06	3.88	4.58e-06	2.61	4.99e-04	1.25
4	3522	6.11e-07	4.03	2.74e-07	4.07	6.27e-05	3.00
4	14082	3.81e-08	4.00	1.69e-08	4.02	7.86e-06	3.00

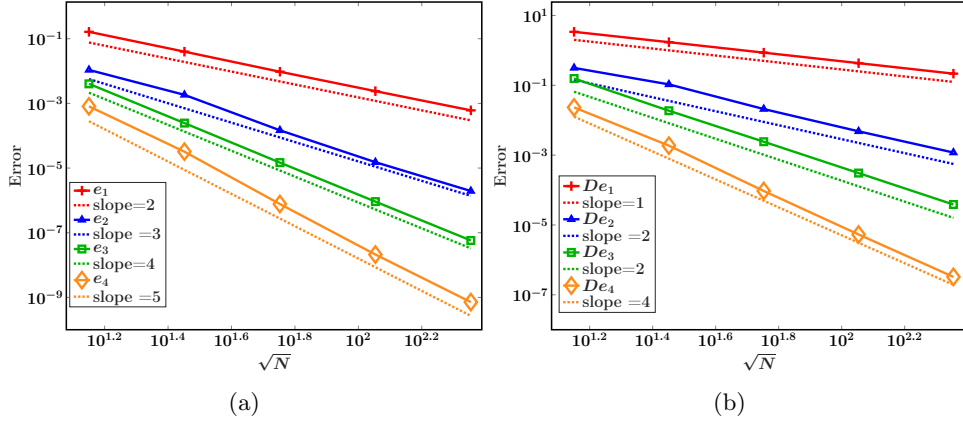


Figure 3: Numerical results of Laplace-Beltrami equation on torus point cloud. (a): L_2 error; (b): H_1 error.

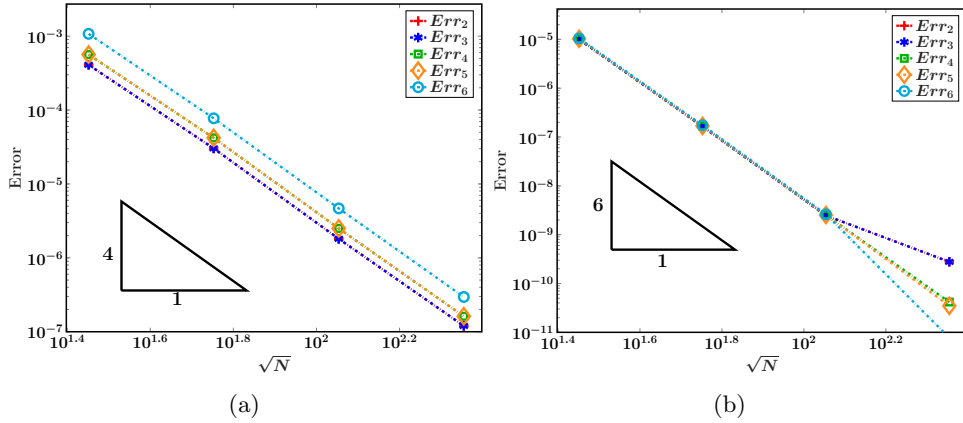


Figure 4: Numerical results of Laplace-Beltrami eigenvalue problem on torus point cloud. (a): $k = l = 2$; (b): $k = l = 4$.

5 Conclusion

In this paper, we have proposed a high-order DG method for numerical solutions of PDEs on point clouds. Our particular focus is on the numerical analysis of this method since existing results in the literature are not applicable in such situations. To do so, we introduced a new error analysis framework for the geometric approximation without exact geometric information and global continuity assumptions. This framework provides a common umbrella to cover existing numerical analysis results on surface Galerkin methods (including both continuous and discontinuous finite elements) in the literature, even though it is implemented for a specific DG method only.

A A proof of Lemma 2.7

Proof. We consider first the case that $p_h^{k,j}$ is produced from interpolation by the polynomial graph, let us denote by $p_h^{*k,j}$. This is when the number m in calculating (2.5) in Algorithm 1 equals to the number of unknown coefficients for determining the polynomial, let us denote it by m^* . Then the above estimate is a direct result from approximation theory. When $m > m^*$, we use the property that $p_h^{k,j}$ is a minimizer of (2.5). It is evident that

$$\sum_{i=1}^m |p^j(r_i^j) - p_h^{k,j}(r_i^j)|^2 \leq \sum_{i=1}^m |p^j(r_i^j) - p_h^{*k,j}(r_i^j)|^2,$$

since $p^j(r_i^j) = \zeta_i^j$ for $i = 1, \dots, m$. We have $|p^j(r_i^j) - p_h^{*k,j}(r_i^j)| \leq Ch^{k+1}$ for all $i = 1, \dots, m$, which indicates that

$$|p^j(r_i^j) - p_h^{k,j}(r_i^j)| \leq C'h^{k+1} \text{ for all } i = 1, \dots, m.$$

We have also that $p_h^{*k,j}$ interpolates p^j . As $p_h^{*k,j}$ and $p_h^{k,j}$ both be k^{th} order local polynomials. Then we can pick m^* points out of the m points, and to have $p_h^{k,j} = \sum_{i=1}^{m^*} p_h^{k,j}(r_i^j)\phi_i$, and $p_h^{*k,j} = \sum_{i=1}^{m^*} p^j(r_i^j)\phi_i$, where $(\phi_i)_{i=1}^{m^*}$ are Lagrange polynomial bases. Since $|p_h^{*k,j}(r_i^j) - p_h^{k,j}(r_i^j)| \leq Ch^{k+1}$, and $|\phi_i| \leq C$ due to our assumption on the distribution of the selected reconstruction points. We have then for all $r \in \Omega_h^j$

$$|p_h^{*k,j}(r) - p_h^{k,j}(r)| \leq \sum_{i=1}^{m^*} |\phi_i(r)| |p_h^{*k,j}(r_i^j) - p_h^{k,j}(r_i^j)| \leq Ch^{k+1}.$$

This gives us the estimate using the triangle inequality

$$|p^j(r) - p_h^{k,j}(r)| \leq |p^j(r) - p_h^{*k,j}(r)| + |p_h^{*k,j}(r) - p_h^{k,j}(r)| = \mathcal{O}(h^{k+1}) \quad \text{for all } r \in \Omega_h^j.$$

Finally, standard argument leads to the estimate on the derivatives (gradient):

$$|\nabla p^j(r) - \nabla p_h^{k,j}(r)| = \mathcal{O}(h^k) \quad \text{for all } r \in \Omega_h^j.$$

□

B Details on the estimate for each terms in (3.21)

Note that the results of Theorem 2.9 are crucial for the estimates here. For the first term in (3.21), we have:

$$\begin{aligned}
& \sum_j \int_{\Omega_h^j} (\nabla \bar{u}_h^{k,l})^\top ((g_h^k)^{-1} - g^{-1}) \nabla \bar{v}_h \sqrt{|g_h^k|} + (\nabla \bar{u}_h^{k,l})^\top g^{-1} \nabla \bar{v}_h \left(\sqrt{|g_h^k|} - \sqrt{|g|} \right) dA \\
& \leq \|g_h^k ((g_h^k)^{-1} - g^{-1})\|_{L^\infty} \left| \sum_j \int_{\Omega_h^j} (\nabla \bar{u}_h^{k,l})^\top (g_h^k)^{-1} \nabla \bar{v}_h \sqrt{|g_h^k|} dA \right| + \\
& \quad \left\| \left(\sqrt{|g_h^k|} - \sqrt{|g|} \right) \sqrt{|g|}^{-1} \right\|_{L^\infty} \left| \sum_j \int_{\Omega_h^j} (\nabla \bar{u}_h^{k,l})^\top g^{-1} \nabla \bar{v}_h \sqrt{|g|} dA \right| \\
& \leq Ch^{k+1} \left(\|u_h^{k,l}\|_{H^1(\hat{\Gamma}_h^k)} \| (T_h^k)^{-1} v_h \|_{H^1(\hat{\Gamma}_h^k)} + \|T_h^k u_h^{k,l}\|_{H^1(\Gamma_h)} \|v_h\|_{H^1(\Gamma_h)} \right) \\
& = \mathcal{O}(h^{k+1}) \|T_h^k u_h^{k,l}\|_{V_h^l} \|v_h\|_{V_h^l},
\end{aligned}$$

where the last inequality is due to the equivalence of the norms of $H^1(\hat{\Gamma}_h^k)$ and $H^1(\Gamma_h)$ and the embedding that $H^1(\Gamma_h) \subset V_h^l$. For the second term, we have

$$\begin{aligned}
& - \sum_{\bar{e}_h \in \bar{\mathcal{E}}_h} \int_{\bar{e}_h} \{ (\nabla \bar{u}_h^{k,l})^\top ((g_h^k)^{-1} (\partial \pi_h^k)^\top n_h - g^{-1} (\partial \pi)^\top n) \} [\bar{v}_h l_{g_h^k}] dE \\
& \leq \left\| \frac{l_{g_h^k}}{l_g} \right\|_{L^\infty} \| ((g_h^k)^{-1} (\partial \pi_h^k)^\top n_h - g^{-1} (\partial \pi)^\top n) \|_{L^\infty} \left| \sum_{\bar{e}_h \in \bar{\mathcal{E}}_h} \int_{\bar{e}_h} \{ |(\nabla \bar{u}_h^{k,l})^\top| \} [\bar{v}_h] l_g dE \right| \\
& \leq Ch^{k+1} \left\| \sqrt{\beta_h}^{-1} \nabla_g T_h^k u_h^{k,l} \right\|_{L^2(\partial \Gamma_h)} \left\| \sqrt{\beta_h} v_h \right\|_{L^2(\partial \Gamma_h)} \\
& = \mathcal{O}(h^{k+1}) \|T_h^k u_h^{k,l}\|_{H^1(\Gamma_h)} \|v_h\|_* = \mathcal{O}(h^{k+1}) \|T_h^k u_h^{k,l}\|_{V_h^l} \|v_h\|_{V_h^l}.
\end{aligned}$$

while the second last relation we used Cauchy–Schwarz inequality, Lemma 3.2, the norm defined in (3.11) and the relation that $\beta_h = \frac{\beta}{h}$. Similarly, for the third term

$$\begin{aligned}
& - \sum_{\bar{e}_h \in \bar{\mathcal{E}}_h} \int_{\bar{e}_h} \{ (\nabla \bar{v}_h)^\top ((g_h^k)^{-1} (\partial \pi_h^k)^\top n_h - g^{-1} (\partial \pi)^\top n) \} [\bar{u}_h^{k,l} l_{g_h^k}] dE \\
& = \mathcal{O}(h^{k+1}) \|v_h\|_{H^1(\Gamma_h)} \|T_h^k u_h^{k,l}\|_* = \mathcal{O}(h^{k+1}) \|v_h\|_{V_h^l} \|T_h^k u_h^{k,l}\|_{V_h^l}.
\end{aligned}$$

The fourth and the fifth term are also quite similar, while we only have to take care of the geometric error contributed by $\left\| \frac{l_{g_h^k}}{l_g} - l_g \right\|_{L^\infty}$ then we will end up with the same estimate of the second and the third ones up to different constants. The rest is quite trivial and we omit the details.

References

- [1] M. Abramowitz and I. A. Stegun. *Handbook of mathematical functions with formulas, graphs, and mathematical tables*, volume 55 of *National Bureau of Standards Applied Mathematics Series*. For sale by the Superintendent of Documents, U.S. Government Printing Office, Washington, D.C., 1964.
- [2] D. Arnold, F. Brezzi, B. Cockburn, L. Marini. Unified analysis of discontinuous Galerkin methods for elliptic problems. *SIAM J. Numer. Anal.*, 39 (2001/02), no. 5, 1749–1779.
- [3] P. Alliez, L. Saboret, and G. Guennebaud. Poisson surface reconstruction. In *CGAL User and Reference Manual*. CGAL Editorial Board, 5.1.1 edition, 2020.
- [4] P. F. Antonietti, A. Buffa, and I. Perugia. Discontinuous Galerkin approximation of the Laplace eigenproblem. *Comput. Methods Appl. Mech. Engrg.*, 195:3483–3503, 2006.

- [5] P. F. Antonietti, A. Dedner, P. Madhavan, S. Stangalino, B. Stinner, and M. Verani. High order discontinuous Galerkin methods for elliptic problems on surfaces. *SIAM J. Numer. Anal.*, 53(2):1145–1171, 2015.
- [6] D.N. Arnold. An interior penalty finite element method with discontinuous elements. *SIAM J. Numer. Anal.*, 19:742–760, 1982.
- [7] T. Aubin. Best constants in the Sobolev imbedding theorem: the Yamabe problem. In *Seminar on Differential Geometry*, volume 102 of *Ann. of Math. Stud.*, pages 173–184. Princeton Univ. Press, Princeton, N.J., 1982.
- [8] I. Babuška and J. Osborn. *Eigenvalue problems*, volume II of *Handbook of Numerical Analysis*. North-Holland, Amsterdam, 1991.
- [9] D. Boffi. Finite element approximation of eigenvalue problems. *Acta Numerica*, 2010:1–120, 2010.
- [10] A. Bonito, A. Demlow, and R. H. Nochetto. Finite element methods for the laplace–beltrami operator. In *Geometric Partial Differential Equations - Part I*, volume 21 of *Handbook of Numerical Analysis*, pages 1 – 103. Elsevier, 2020.
- [11] A. Bonito, A. Demlow, and J. Owen. A priori error estimates for finite element approximations to eigenvalues and eigenfunctions of the Laplace–Beltrami operator. *SIAM J. Numer. Anal.*, 56(5):2963–2988, 2018.
- [12] K. Deckenlück, G. Dziuk, and C. M. Elliott. Computation of geometric partial differential equations and mean curvature flow. *Acta Numer.*, 14:139–232, 2005.
- [13] A. Dedner and P. Madhavan. Adaptive discontinuous Galerkin methods on surfaces. *Numer. Math.*, 132(2):369–398, 2016.
- [14] A. Dedner, P. Madhavan, and B. Stinner. Analysis of the discontinuous Galerkin method for elliptic problems on surfaces. *IMA J. Numer. Anal.*, 33(3):952–973, 2013.
- [15] A. Demlow. Higher-order finite element methods and pointwise error estimates for elliptic problems on surfaces. *SIAM J. Numer. Anal.*, 47(2):805–827, 2009.
- [16] D. A. Di Pietro and A. Ern. *Mathematical aspects of discontinuous Galerkin methods*, volume 69 of *Mathématiques & Applications (Berlin) [Mathematics & Applications]*. Springer, Heidelberg, 2012.
- [17] G. Dong and H. Guo. Parametric polynomial preserving recovery on manifolds. *SIAM J. Sci. Comput.*, 42(3):A1885–A1912, 2020.
- [18] G. Dong and H. Guo. Superconvergence of differential structure on manifolds and its applications. *arXiv preprint*, pages 1–18, 2020.
- [19] Q. Du and L. Ju. Finite volume methods on spheres and spherical centroidal Voronoi meshes. *SIAM J. Numer. Anal.*, 43(4):1673–1692 (electronic), 2005.
- [20] G. Dziuk. Finite elements for the Beltrami operator on arbitrary surfaces. In *Partial differential equations and calculus of variations*, volume 1357 of *Lecture Notes in Math.*, pages 142–155. Springer, Berlin, 1988.
- [21] G. Dziuk and C. M. Elliott. Finite elements on evolving surfaces. *IMA J. Numer. Anal.*, 27:262–292, 2007.
- [22] G. Dziuk and C. M. Elliott. Finite element methods for surface PDEs. *Acta Numer.*, 22:289–396, 2013.
- [23] J. Grande and C. Lehrenfeld and A. Reusken. Analysis of a high-order trace finite element method for PDEs on level set surfaces. *SIAM J. Numer. Anal.*, 56(1):228–255, 2018.

- [24] H. Guo. Surface Crouzeix-Raviart element for the Laplace-Beltrami equation. *Numer. Math.*, 144(3):527–551, 2020.
- [25] Jan S. Hesthaven and Tim Warburton. *Nodal discontinuous Galerkin methods*, volume 54 of *Texts in Applied Mathematics*. Springer, New York, 2008. Algorithms, analysis, and applications.
- [26] M. Kazhdan, M. Bolitho, and H. Hoppe. Poisson Surface Reconstruction. In Alla Sheffer and Konrad Polthier, editors, *Symposium on Geometry Processing*. The Eurographics Association, 2006.
- [27] M. Kazhdan, H. Hoppe, Screened poisson surface reconstruction. *ACM Transactions on Graphics (ToG)*, 32(3), 1-13, 2013.
- [28] Z. Li and Z. Shi. A convergent point integral method for isotropic elliptic equations on a point cloud. *Multiscale Modeling and Simulation*, 14(2):874–905, 2016.
- [29] J. Liang and H. Zhao. Solving partial differential equations on point clouds. *SIAM J. Sci. Comput.*, 35(3):A1461–A1486, 2013.
- [30] W. Lu, Z. Shi, B. Wang and J. Sun Surface Reconstruction Based on Modified Gauss Formula. *Transactions on Graphics*, 38(1):1-18, 2018.
- [31] M. A. Olshanskii, A. Reusken, and J. Grande. A finite element method for elliptic equations on surfaces. *SIAM J. Numer. Anal.*, 47(5):3339–3358, 2009.
- [32] Béatrice Rivière. *Discontinuous Galerkin methods for solving elliptic and parabolic equations*, volume 35 of *Frontiers in Applied Mathematics*. Society for Industrial and Applied Mathematics (SIAM), Philadelphia, PA, 2008. Theory and implementation.
- [33] H. Wendland. *Scattered Data Approximation*, volume 17 of *Cambridge Monographs on Applied and Computational Mathematics*. Cambridge University Press, first edition, 2005.